ORGAN NEEDLE PLUTON, NEW MEXICO: INCREMENTALLY EMPLACED FROM DEEP CRUSTAL SOURCES

Kathleen Marie Wooton

A thesis submitted to the faculty at the University of North Carolina at Chapel Hill in partial fulfillment of the requirements for the degree of Master of Science in the Department of Geological Sciences in the College of Arts and Sciences.

Chapel Hill
2014

Approved by:

Drew S. Coleman

Allen F. Glazner

Jonathan M. Lees

ABSTRACT

Kathleen Marie Wooton: Organ Needle Pluton, New Mexico:
Incrementally Emplaced from Deep Crustal Sources
(Under the direction of Drew S. Coleman)

The zoned Organ Needle Pluton is associated with three silicic ignimbrites. Precise $^{206}Pb/^{238}U$ zircon TIMS ages indicate the pluton was assembled from the top downward, with the most silicic compositions having the oldest ages. The most mafic compositional phase of the pluton, a monzodiorite was emplaced during a discrete episode after the alkali feldspar granite and inequigranular syenite. The tuff of Squaw Mountain and alkali feldspar granite could not have been derived by fractional crystallization and crystal separation from the inequigranular syenite and monzodiorite.

These new age relations suggest the isotopic variation within the Organ Needle Pluton initially reflects assimilation of local Precambrian quartz monzonite. As magma emplacement into the region continued, the magma system self buffered, recording a consistent, less-evolved isotopic signature of a single magma source. Furthermore, $^{206}Pb/^{238}U$ zircon crystallization ages indicate the pluton was emplaced in a younger, separate event from the magmatism that generated the ignimbrites.

TABLE OF CONTENTS

LIST OF TABLES

LIST OF FIGURES

LIST OF ABBREVIATIONS

a	annum
abs	absolute
FCT	Fish Canyon Tuff
ID-TIMS	isotope-dilution thermal ionization mass spectrometry
ka	kilo-annum
KS test	Kolmogorov-Smirnov test
LA ICP-MS	laser ablation inductively coupled plasma mass spectrometry
Ma	mega-annum
MIT	Massachusetts Institute of Technology
MSWD	mean square weighted deviate
mtn.	mountain
NAD	North American Datum
Pb*	radiogenic Pb
Pbc	common Pb
pg	picogram
ppm	parts per million
qtz	quartz
T-t	temperature – time
wt.%	weight percent
UNC	University of North Carolina
UTM	Universal Transverse Mercator

Introduction

Volcanic rocks provide an instantaneous view of lithospheric magma systems, and the integrated history of a volcanic system provides a time series of its chemical evolution (Lipman et al., 1966; Hildreth, 1979; Lipman, 2007). Spatial and chemical similarities between large silicic ignimbrites and large silicic plutons led to the interpretation that plutons represent the crystallized final phase of large, liquid magma chambers beneath volcanic fields (Smith, 1960; Hildreth, 1979; Hildreth, 1981; Lipman, 1984). As such, magma evolution processes (e.g., crystal settling, wall rock assimilation) founded on chemical variations observed in volcanic suites were developed that require a large, mostly liquid (~40-50% crystals) magma chamber (Lipman et al., 1966; Hildreth, 1981; Bachmann et al., 2007; Hildreth and Wilson, 2007; Lipman, 2007). However, the existence of sustained, large, upper crustal, liquid magma chambers, a supposition underlying igneous petrology for the last 50 years, has recently been called into question (Coleman et al., 2004; Glazner et al., 2004). High-precision geochronology on granitic batholiths indicate that plutons are incrementally emplaced in the upper crust as small magma batches over several Ma (Coleman et al., 2004; Glazner et al., 2004; Hirt, 2007; Tappa et al., 2011; Davis et al., 2012). Additionally, conservative thermal modeling of upper crustal magma bodies indicate that batholiths should cool and crystallize in only a few 100 ka, before processes like fractional crystallization and compositional zonation can become effective (Coleman et al., 2004; Glazner et al., 2004; Annen, 2009; Schöpa and Annen, 2013). Geophysical research also suggests that a large, mostly liquid magma model is not supported by the data (Lees,

2007). Imaging the structure of magma systems beneath active volcanoes (Lees, 1992; Moran et al., 1999; Masturyono et al., 2001; Lees, 2007; Agostinetti and Chiarabba, 2008), consistently suggests that the low-velocity structures beneath volcanoes reflect maximum melt compositions of only ~20% (Iyer, 1979; Schilling and Partzsch, 2001).

Compositionally zoned ignimbrites and plutons are commonly interpreted as having evolved within a chemically stratified magma system (e.g., Topopah Spring Tuff, Nevada: Lipman et al., 1966; Tuolumne Intrusive Suite, California: Bateman and Chappell, 1979; Bishop Tuff, California: Hildreth and Wilson, 2007). Normally zoned ignimbrites grade from high or low-silica rhyolite at their base into dacitic tuff at the top (Lipman et al., 1966; Hildreth, 1979; Seager, 1981; Lipman, 2007). The preferred geochemical model for producing zoned ignimbrites is the evacuation of a stratified magma system from the top down, first erupting a silicic cap, followed sequentially by more mafic magmas (Smith and Bailey, 1965; Hildreth, 1979). Thus, U-Pb geochronology of zircons from a compositionally zoned magma system should be expected to reflect the differentiation of a fractionating system, with the cooling and crystallization of deeper mafic magmas preceding the solidification of shallower silicic magmas. However, Tappa et al., (2011) observed a top-down emplacement history for the Rio Hondo pluton (Latir volcanic field, New Mexico). The silicic cap of the system intruded first, in the shallow crust, with successively more mafic units intruded later below at greater depths (Tappa et al., 2011). They propose that the chemical variation within zoned plutons and ignimbrites is characteristic of lower crustal source magmas and unrelated to chemical evolution in the upper crust (Coleman et al., 2004; Tappa et al., 2011; Coleman et al., 2012).

It is important to thoroughly evaluate these traditional and newer alternative magma evolution processes in order to reconcile new observations with an evolving understanding of igneous petrology. The Organ Mountains near Las Cruces, New Mexico, provide the opportunity to directly study both the volcanic and plutonic rocks of a large, silicic magma system. The chemically zoned tuff of Squaw Mountain and Organ Needle Pluton have been studied and a detailed geochemical model exists for the evolution of the Organ Needle Pluton (Dunham, 1935; Seager and Brown, 1978; Seager, 1981; Seager and McCurry, 1988; Butcher et al., 1989; Verplanck et al., 1995, 1999). Existing geochronologic data support the geochemical model that the Organ Needle Pluton evolved by fractional crystallization and crystal separation, with the youngest unit being the most silicic of the plutonic suite (Rioux et al., 2010). A few, imprecise ages suggest a more complex emplacement history for the Organ Needle Pluton (Zimmerer and McIntosh, 2013).

The Organ Mountains

The Organ Mountains are located on the southeastern edge of the Mogollon-Datil Volcanic Field and preserve the remnants of a large silicic, caldera-forming volcanic system, the Organ Caldera and the Organ Batholith (Dunham, 1935; Seager, 1981). Three ignimbrites erupted from the Organ Caldera – the aphyric, high-silica Cueva Tuff (77 wt.% SiO_2, 36.45 ± 0.08 Ma, $^{40}Ar/^{39}Ar$ sanidine ages calculated using FCT = 28.201 Ma, all Ar-age uncertainties reported to 2σ and do not include ^{40}K decay constant uncertainty) and tuff of Achenback Peak (75-74 wt.% SiO_2, 36.23 ± 0.14 Ma), and the compositionally zoned tuff of Squaw Mountain (72-68 wt.% SiO_2, 36.03 ± 0.16 Ma, Figure 1, Seager and Brown, 1978; Seager and McCurry, 1988; Zimmerer and McIntosh, 2013). The tuff of Squaw Mountain is

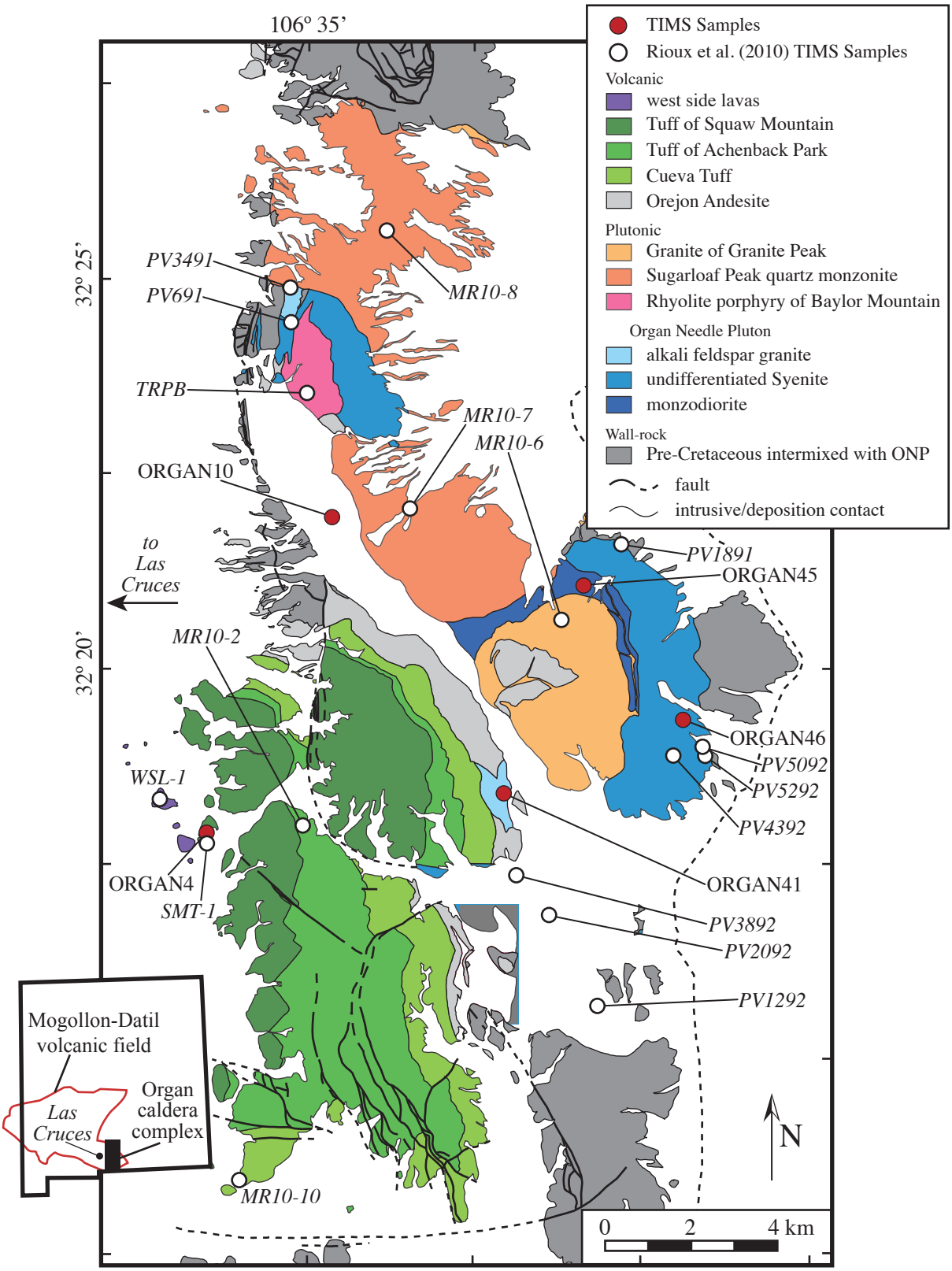

Figure 1. Geologic map of the Organ Mountains in New Mexico, USA, after Seager (1981) and Verplanck et al. (1999). Sample locations for this study are indicated by red circles. Samples of Rioux et al. (2010) are indicated by white circles and italicized identifiers.

normally zoned, ranging from crystal-poor high-silica rhyolite at the base to crystal-rich dacite at the top (Seager, 1981; Seager and McCurry, 1988).

Pluton intrusion into the overlying Precambrian crystalline basement, thick Paleozoic sedimentary sequences, and the Eocene Orejon Andesite began with the compositionally zoned Organ Needle Pluton (Figure 1, Dunham, 1935; Seager and Brown, 1978; Seager, 1981). Igneous activity continued with decreased volcanism and the intrusion of the granite of Granite Peak, the Sugarloaf Mountain monzonite, and the Baylor Mountain rhyolite porphyry (Figure 1, Seager, 1981; Seager and McCurry, 1988). During the late Tertiary, the Organ Batholith was uplifted and tilted west 15-20° by faulting associated with the Rio Grande Rift (Seager, 1981; Seager and McCurry, 1988; Chapin et al., 2004). The Organ Mountains provide exposure of the Organ Needle Pluton across 6 km of paleodepth (Verplanck et al., 1995). The remnants of the Organ Caldera and its three ignimbrites are exposed on the western side of the Organ Mountain range and in the northern and eastern regions of the mountains, a portion of the Organ Needle Pluton and younger intrusions underlying the volcanic field are exposed (Figure 1, Dunham, 1935; Seager, 1981; Chapin et al., 2004).

Geochemistry of the Organ Needle Pluton

Though dominantly equigranular syenite, the Organ Needle Pluton includes four petrographically distinct phases: alkali feldspar granite, equigranular quartz syenite, inequigranular syenite, and monzodiorite (Seager, 1981; Seager and McCurry, 1988; Verplanck et al., 1995, 1999). Contacts between these phases are generally gradational and the individual phases are compositionally variable. The most silicic plutons are exposed at the highest structural levels, and the plutons become more mafic with paleodepth (Seager and

McCurry, 1988; Verplanck et al., 1995). Rounded mafic enclaves are common throughout the pluton (Seager, 1981; Verplanck et al., 1995, 1999).

The course-grained, equigranular quartz syenite ranges from quartz syenite to monzodiorite, and its major and trace element geochemistry show systematic variation with structural depth (Verplanck et al., 1995, 1999). The equigranular quartz syenite is isotopically uniform with both whole rock and mineral separates having an $\varepsilon_{Nd} = -2$ and $^{87}Sr/^{86}Sr_i = 0.706$ (Verplanck et al., 1995, 1999).

A course-grained, inequigranular syenite that ranges in composition from alkali feldspar granite to monzodiorite forms a thin border around the equigranular quartz syenite (Figure 1; Verplanck et al., 1995, 1999). The inequigranular syenite contains restitic xenoliths of the local Precambrian White Sands quartz monzonite that are not present in any of the other mapped units (Condie and Budding, 1979; Verplanck et al., 1995, 1999). Generally, the inequigranular syenite has a positive Eu-anomaly and is enriched in rare earth elements compared to the equigranular syenite (Verplanck et al., 1995, 1999). However, the inequigranular syenite shows no systematic variation in trace element concentration or isotopic composition with major element trends or depth (Verplanck et al., 1995, 1999). It does have a large isotopic range with ε_{Nd}-values from -3.2 to -5.5 (generally, <-4.5) and $^{87}Sr/^{86}Sr_i$ from 0.7075 to 0.7191 (generally, $^{87}Sr/^{86}Sr_i > 0.709$; Verplanck et al., 1995, 1999). As with the equigranular quartz syenite though, there is no significant difference in ε_{Nd} from whole rock and mineral separates (Verplanck et al., 1999). The presence of restitic xenoliths and mafic enclaves with $\varepsilon_{Nd} = -2$ in the inequigranular syenite suggest the inequigranular syenite is cogenic with the equigranular quartz syenite (Verplanck et al., 1999). Assimilation

of ~20% quartz monzonite (average ε_{Nd} = -12.1 for White Sands) could produce an ε_{Nd} = -5 magma from the equigranular quartz syenite (Verplanck et al., 1999).

Along the western contact of the Organ Needle Pluton, the highest exposed structural level of the pluton, are several isolated cupolas of fine to medium-grained alkali feldspar granite (Figure 1; Seager, 1981; Seager and McCurry, 1988; Verplanck et al., 1995, 1999). The alkali feldspar granite is interpreted as the plutonic equivalent of the tuff of Squaw Mountain because they share similar whole-rock and isotope geochemistry (Butcher et al., 1989; Verplanck et al., 1995). The alkali feldspar granite has ε_{Nd} = -5 and $^{87}Sr/^{86}Sr_i > 0.709$ (Verplanck et al., 1995).

The interior of the southern portion of the Organ Needle Pluton is monzodiorite (Figure 1; Dunham, 1935; Seager, 1981). The monzodiorite is isotopically uniform with ε_{Nd} = -3.5 and $^{87}Sr/^{86}Sr_i$ = 0.706 (Verplanck et al., 1995, 1999).

Verplanck et al. (1995, 1999) interpreted the Organ Needle Pluton as a composite of two separately evolving, coeval magmas – the first with an ε_{Nd}–signature of -2 and the second with an ε_{Nd}–signature of -5. Initially, a -2 ε_{Nd} mafic magma was emplaced, evolving by fractional crystallization and magma migration, forming the chemically gradational equigranular quartz syenite (Verplanck et al., 1995, 1999). Concurrently, a second magma (possibly the residual of the equigranular quartz syenite magma) evolved by assimilation of local basement rocks, fractional crystallization and crystal separation (Verplanck et al., 1995, 1999). It then migrated in small batches along the margin of the equigranular quartz syenite, forming a chemically zoned outer shell around the equigranular quartz syenite – an alkali feldspar granite cap, an inequigranular syenite border, and a monzodiorite base (Verplanck et

al., 1995, 1999). The tuff of Squaw Mountain erupted from the rising alkali feldspar granite magmas (Butcher et al., 1989; Verplanck et al., 1995).

Geochronology of the Organ Needle Pluton

Initial dating of the Organ Caldera and Batholith indicated that the ignimbrites and the Organ Needle Pluton were contemporaneous within resolution at ~35.7 Ma (Verplanck et al., 1995). Isotope-dilution thermal ionization mass spectrometry (ID-TIMS) U-Pb zircon geochronology indicates the equigranular quartz syenite and inequigranular syenite were emplaced between ~36.3-36.1 Ma and the alkali feldspar granite is significantly younger (~35.2-35.1 Ma, Rioux et al., 2010). The zircon $^{206}Pb/^{238}U$ crystallization age of the overlying West Side lavas establishes the minimum age of the tuff of Squaw Mountain as ~35.6 Ma, suggesting that it is older and unrelated to the alkali feldspar granite of the Organ Needle Pluton (Rioux et al., 2010). Newer geochronologic data including both $^{40}Ar/^{39}Ar$ and laser ablation inductively coupled plasma mass spectrometry (LA ICP-MS) U-Pb geochronology support the conclusions of Rioux et al., (2010), except they indicate an older crystallization age for the alkali feldspar granite sample (Zimmerer and McIntosh, 2013). The collection sites of the alkali feldspar granite samples collected in these studies are separated by several km, and Zimmerer and McIntosh (2013) suggest these samples represent two separate alkali feldspar granite emplacement events: an older episode of magmatism related to Organ Needle Pluton emplacement in the southern mountains (36.48 ± 0.62 Ma, Zimmerer and McIntosh, 2013) and a younger event in the northern Organ Mountains (~35.2-35.1 Ma, Rioux et al., 2010). Their LA ICP-MS U-Pb zircon ages have large uncertainties (ranging from 0.6 to 2 Ma, Zimmerer and McIntosh, 2013). Although all of the Organ Needle Pluton ages overlap within uncertainty (with ages from ~36.5-34.9 Ma), the LA ICP-MS zircon U-

Pb age of the equigranular quartz syenite is noticeably younger than the other Organ Needle Pluton phases (Zimmerer and McIntosh, 2013). Zimmerer and McIntosh (2013) dismiss the equigranular quartz syenite zircon age in favor of an older $^{40}Ar/^{39}Ar$ biotite age, attributing the young $^{206}Pb/^{238}U$ age to Pb loss. They conclude that the entire Organ Needle Pluton was emplaced simultaneously during local ignimbrite eruption, and accordingly, the Organ Needle Pluton alkali feldspar granite is contemporaneous and cogenetic with the tuff of Squaw Mountain (Zimmerer and McIntosh, 2013). Finally, biotite cooling ages suggest that the Organ Needle Pluton cooled quickly (<0.5 Ma). Multiple diffusion domain modeling of K-feldspar step-heating age spectra suggest thermal perturbations within the Organ Needle Pluton at 35-34 Ma, 32-30 Ma and 28-25 Ma (Zimmerer and McIntosh, 2013).

The low precision associated with Zimmerer and McIntosh's (2013) LA ICP-MS zircon ages is problematic for detailed interpretation of the Organ Needle Pluton T-t history. For only the Organ Needle Pluton and related ignimbrites, the resolution of their thermochronology is too broad to distinguish age relationships between plutonic phases, as well as, those between the Organ Needle Pluton phases and each individual ignimbrite (Tappa et al., 2011; Mills and Coleman, 2013; Rosera et al., 2013). Additionally, as noted by the authors, there is a T-t conflict between the equigranular quartz syenite $^{206}Pb/^{238}U$ ages and $^{40}Ar/^{39}Ar$ ages (Zimmerer and McIntosh, 2013). Their preferred biotite age indicates cooling below ~350°C around 36 Ma, while the zircon ages suggest the equigranular quartz syenite crystallized 1 Ma later at temperatures (~800°C) that would have reset the pluton's K-Ar system to a maximum of ~35 Ma (Harrison et al., 1985; McDougall and Harrison, 1999; Harrison et al., 2007).

The recent geochronologic work on large silicic plutons has altered our understanding of pluton formation, setting aside the model of emplacement and cooling as a single magmatic body in favor of incremental emplacement of small batches of magma over time periods of more than 100 ka to several Ma (Coleman et al., 2004; Tappa et al., 2011; Davis et al., 2012). With this new outlook, the study of plutons requires analysis of multiple samples from across individual plutons, with datasets comparable only within a single sample location (Coleman et al., 2004; Davis et al., 2012; Rosera et al., 2013). Multiple techniques (e.g., $^{206}Pb/^{238}U$, $^{40}Ar/^{39}Ar$) must analyze the same sample to account for this extended emplacement history. This dilemma is highlighted by the age difference between the southern and northern exposures of the Organ Needle Pluton alkali feldspar granite (Rioux et al., 2010; Zimmerer and McIntosh, 2013; this study). Zircons from the Organ Needle Pluton and tuff of Squaw Mountain samples of Zimmerer and McIntosh (2013) were analyzed by chemical abrasion ID-TIMS for $^{206}Pb/^{238}U$ geochronology in order to remove the uncertainty associated with the incremental emplacement. These new U-Pb ages resolve subtle age differences between the different chemical phases of the Organ Needle Pluton and provide precise zircon crystallization ages to support the thermochronology of Zimmerer and McIntosh (2013).

Methods

Zimmerer and McIntosh (2013) collected and analyzed 32 samples from the Organ Mountains, near Las Cruces, New Mexico, using $^{40}Ar/^{39}Ar$ thermochronology. Samples of the four compositional phases of the Organ Needle Pluton and a sample of the tuff of Squaw Mountain were selected for further analysis using U-Pb zircon geochronology. Zircon mineral separates for these five samples were prepared using standard techniques, including a shaking water separation table and Frantz magnetic separation. Intact and generally

inclusion-free zircons were hand picked from each sample. These zircons were then thermally annealed for 48 hours at 950°C and chemically abraded with hydrofluoric acid for 16 hours at 220-230°C (Mundil et al., 2004; Mattinson, 2005). Aliquots of individual zircons or groups of 2 to 4 zircons were then cleaned, dissolved, and processed through anion-exchange chromatography following procedures similar to Parrish et al. (1987). Prior to dissolution, each aliquot was spiked with a ^{205}Pb-^{233}U-^{236}U tracer (Parrish and Krogh, 1987). These aliquots were then analyzed by ID-TIMS at the UNC Geochronology and Isotope Geochemistry Laboratory, Chapel Hill, North Carolina.

Uranium-Pb data for all analyses were reduced using U-Pb Redux (McLean et al., 2011) assuming no initial Pb was present. Because the Organ Needle Pluton is relatively young (<100 Ma), all analyses were Th-corrected (Mattinson, 1973; Schärer, 1984). Estimates of Th/U for each unit were established using the average U and Th concentration of similar Organ Needle Pluton samples (Verplanck et al., 1999). Sample names correspond to the names used by Zimmerer and McIntosh (2013).

Results

Zircon $^{205}Pb/^{238}U$ dates for the equigranular quartz syenite ranged from 88.0 Ma to 15.5 Ma, but the majority of analyses spread from 35.4 Ma and 34.9 Ma. For the inequigranular syenite, zircon dates range from 36.3 Ma to 35.7 Ma. For zircons from the alkali feldspar granite, the $^{205}Pb/^{238}U$ dates range from 37.2 Ma to 33.6 Ma, with most analyses falling between 36.7 Ma and 36.1 Ma. Zircon analyses from the monzodiorite were all within uncertainty of one another and ranged from 36.12 Ma and 36.04 Ma.

Zircons from the tuff of Squaw Mountain have low U-concentrations (averaging 7.9 pg of Pb* vs. 76.8 pg average in inequigranular syenite zircons). Zircon $^{205}Pb/^{238}U$ dates range

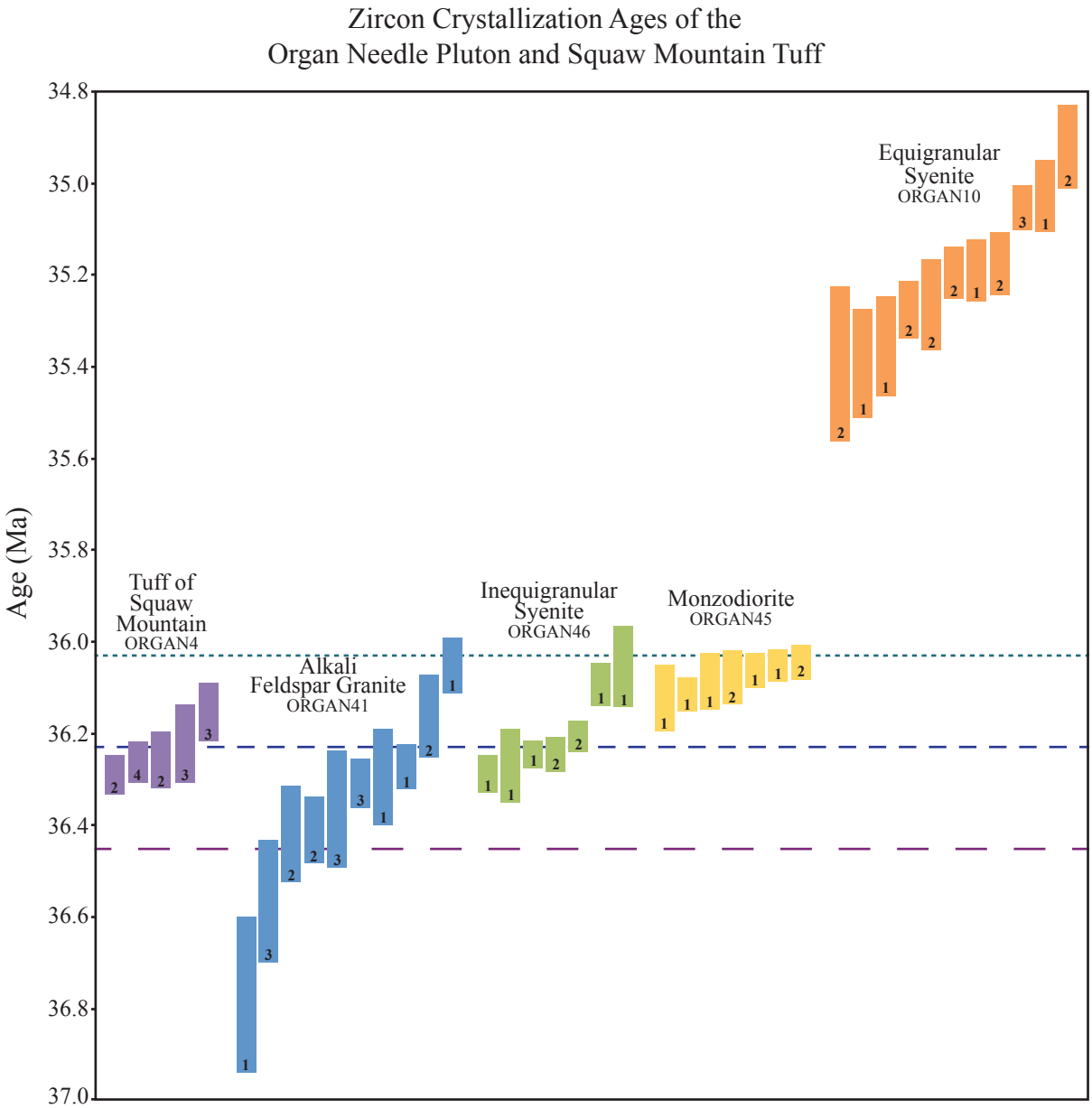

Figure 2. $^{206}Pb/^{238}U$ zircon crystallization ages for the equigranular quartz syenite (sample no. ORGAN10), alkali feldspar granite (ORGAN41), monzodiorite (ORGAN45), and inequigranular syenite (ORGAN46) phases of the Organ Needle Pluton and for the base of tuff of Squaw Mountain (ORGAN4). Each bar represents a single TIMS analysis with 2σ uncertainty. Number at base of each bar indicates number of zircons within each aliquot. Ages given for the Cueva, Achenback Park, and Squaw Mountain tuffs are $^{40}Ar/^{39}Ar$ eruption ages from Zimmerer and McIntosh (2013).

from 40.3 Ma to 32.9 Ma, with the majority of analyses clustering between 36.9 Ma and 35.5 Ma.

Discussion

These new $^{206}Pb/^{238}U$ zircon ages require review of the petrogenetic model for the Organ pluton and volcanic field. This reevaluation provides insight into the formation of compositionally zoned plutons and their relation to chemically zoned ignimbrites. Finally, comparison of these zircon ages to those of Rioux et al. (2010) lends a better understanding of the intrusion history of the Organ region.

Zircon Crystallization Ages

A multigrain approach was adopted in analyzing zircons from the tuff of Squaw Mountain and the Organ Needle Pluton because of low U concentrations in individual zircons. This increases the Pb* yield per analysis, however, it potentially could lead to precise but inaccurate dates. Zircons with Pb-loss or inheritance issues could be included in the pooled isotopic data leading to incorrect dates or a spread in ages for an extended zircon crystallization could be reduced by averaging isotopic data. However, the pooling of isotopic data of significantly dissimilar ages should produce discordant dates. Additionally, chemical abrasion has been satisfactorily shown to remove damaged zircon crystal lattice and eliminate concerns over Pb-loss (Mundil et al., 2004; Mattinson, 2005). The use of chemical abrasion prior to analysis and careful removal of discordant and unreasonable data should not bias the results of this study, and should allow for data comparable to those of Rioux et al. (2010; who completed only single-grain analyses) and future researchers.

After zircon analyses with unreasonably large uncertainties were removed from the data ($2\sigma > 200$ ka), the $^{206}Pb/^{238}U$ zircon ages for the equigranular quartz syenite, the alkali

feldspar granite, the inequigranular syenite, and the monzodiorite of the Organ Needle Pluton exhibit a normal distribution in ages (Figure 2). Four outliers, with ages of more than 1 Ma difference from all other analyses in their respective sample, were removed from the data sets and not included in data analysis (F-4, 34.96 Ma, from the alkali feldspar granite, F-6, 15.46 Ma, F-3, 31.13 Ma, and F-7, 79.74 Ma from the equigranular quartz syenite). These removed data indicate both inheritance and Pb-loss is present within the zircons of the equigranular quartz syenite (along with the two outliers, two other analyses were removed for large uncertainty, F-6, 15.46 Ma, and F-17, 87.99 Ma). Two other outliers were removed at the author's discretion from the data sets and further data analysis for Pb-loss and inheritance (F-9, 37.23 Ma, from the alkali feldspar granite, F-5, 35.67 Ma, from the inequigranular syenite).

The tuff of Squaw Mountain zircons have very low U-concentrations and after removal of zircon analyses with large uncertainties ($2\sigma > 200$ ka), the $^{206}Pb/^{238}U$ zircon ages do not represent a normal distribution of ages. One analysis, F-8, 35.52 Ma, is significantly younger than the $^{40}Ar/^{39}Ar$ eruption age for the tuff (Zimmerer and McIntosh, 2013) and was removed from the dataset due to interpreted Pb-loss. Two other analyses were removed from the data at the author's discretion for large uncertainties and significant separation from the remaining data suggesting possible Pb-loss and inheritance within these zircons (F-1, 35.81 Ma and F-11, 36.89 Ma). The tuff of Squaw Mountain data does statistically represent a normal distribution in population after the removal of these three analyses (Figure 2).

Statistically, the $^{206}Pb/^{238}U$ zircon ages of the compositional phases of the Organ Needle Pluton and the tuff of Squaw Mountain are likely to represent a normal population, however, the small number of analyses per sample produces conflicting statistical population indictors

Table 1. $^{206}Pb/^{238}U$ zircon ages for the Organ Needle Pluton and the tuff of Squaw Mountain.

Unit	Sample	$^{206}Pb/^{238}U$ Age (Ma)
Alkali Feldspar Granite	ORGAN41	36.77 ± 0.17 (±0.18) to 36.052 ± 0.061 (±0.074) [*] **36.285 ± 0.024** (±0.049) [†]
Inequigranular Syenite	ORGAN46	36.245 ± 0.017 (0.044) & **36.085 ± 0.041** (0.058) [‡] 36.221 ± 0.016 (±0.044) [†]
Monzodiorite	ORGAN45	**36.072 ± 0.016** (±0.044) [†]
Equigranular Quartz Syenite	ORGAN10	35.39 ± 0.17 (±0.17) to 34.919 ± 0.091(±0.10) [*] **35.162 ± 0.022** (±0.047) [†]
Tuff of Squaw Mountain	ORGAN4	36.293 ± 0.043 (±0.061) to 36.155 ± 0.062 (±0.075) [*] **36.253 ± 0.024** (±0.048) [†]

[*] Range of $^{206}Pb/^{238}U$ zircon TIMS ages with analytical uncertainty and, in parentheses, uncertainty including error associated with the ^{205}Pb-^{233}U-^{236}U tracer and the ^{238}U decay constant.

[†] Weighted mean age of $^{206}Pb/^{238}U$ zircon ages.

[‡] Weighted mean ages of individual age clusters of inequigranular syenite $^{206}Pb/^{238}U$ zircon ages (analyses F-3, F-4 F-6 to F-8, and analyses F-1 and F-2, respectively).

for these samples and it is possible that there is non-analytic scatter represented in the age distributions. The mean square weighted deviate (MSWD) is used to interpret geologic scatter within the age distributions for samples with less than 10 analyses (Wendt and Carl, 1991; Mahon, 1996). The equigranular quartz syenite and alkali feldspar granite have a sufficiently large enough data set ($n \geq 10$) to allow for statistical robustness of Kolmogorov-Smirnov tests (KS tests) to determine their age population distributions. The weighted mean of normally distributed age populations is interpreted as the age of magma emplacement within the upper crust and commencement of zircon crystallization as that magma cooled to around 800°C (Harrison et al., 2007).

Kolmogorov-Smirnov tests indicate both the equigranular quartz syenite and alkali feldspar granite age populations are representative of a normal distribution. The weighted mean age for the equigranular quartz syenite is 35.162 ± 0.022 Ma (n=11, MSWD=11, Table

1). The range of these analyses is 35.392 to 34.919 Ma (Figure 2). The weighted mean age the alkali feldspar granite is 36.285 ± 0.024 Ma (n=10, MSWD=15, Table 1). The range of the alkali feldspar granite ages is 36.771 to 36.052 Ma (Figure 2). This study interprets the $^{206}Pb/^{238}U$ weighted mean ages for the equigranular quartz syenite and alkali feldspar granite as the age of magma emplacement into the upper crust. It is possible, however, that the ages represent extended zircon crystallization and cooling of these two plutons.

The MSWD statistics are preferable to a KS test for the inequigranular syenite ages. The weighted mean age of inequigranular syenite zircon analyses is 36.221 ± 0.016 Ma and has an MSWD of 10 (n=7, Table 1). The inequigranular syenite data appear to represent two discrete populations (Figure 2): two younger analyses have a weighted mean age of 36.085 ± 0.041 Ma, with the rest of the data clustering around an older weighted mean age of 36.245 ± 0.017 Ma (MSWD = 2.4). The two weighted mean ages are interpreted as representing two discrete periods of zircon crystallization preserved within the inequigranular syenite. The older zircons are likely antecrysts within the inequigranular syenite (Charlier et al., 2005; Miller et al., 2007) and so, the youngest two analyses are interpreted as the emplacement age of the inequigranular syenite within the upper crust.

The weighted mean age of 7 analyses from the monzodiorite is 36.072 ± 0.016 Ma with a MSWD of 1.9 (Table 1). The zircon ages from the monzodiorite do not exhibit geologic scatter and represent a discrete population (Figure 2). The weighted mean age of the monzodiorite analyses is interpreted as representing a single, distinct period of zircon crystallization and as the age of magma emplacement within the upper crust of the monzodiorite.

Although the tuff of Squaw Mountain zircon ages are statistically representative of a normal population, the data does appear to exhibit geologic scatter. The $^{206}Pb/^{238}U$ weighted mean age for the tuff of Squaw Mountain is 36.253 ± 0.024 Ma with an MSWD = 3.5 (n = 5, Table 1). The zircon ages for the tuff range from 36.293 to 36.155 Ma (Figure 2). The $^{206}Pb/^{238}U$ weighted mean age is cautiously interpreted as a single period of zircon crystallization reflecting cooling of the parent magma to around 800°C (Harrison et al., 2007). The minimum age for the tuff cooling below 800°C is the youngest zircon age of 36.155 ± 0.062 Ma (Figure 2). Both the weighted mean age and the minimum cooling age are within uncertainty of the $^{40}Ar/^{39}Ar$ eruption age for the tuff (Zimmerer and McIntosh, 2013).

Although the equigranular quartz syenite dated in this study is almost 1 Ma younger than the other Organ Needle Pluton phases (Figure 2), patterns in the thermal history (see below) of the Organ Mountains suggest this relationship is a product of sample location. The alkali feldspar granite, inequigranular syenite and monzodiorite samples are located in close proximity to one another in the central Organ Mountains, but the younger equigranular quartz syenite sample is located over 5 km away in the northern mountains (Figure 1). Analyzing the $^{206}Pb/^{238}U$ ages of a sample of equigranular quartz syenite in the southern Organ Mountains may result in zircon crystallization ages closer to 36 Ma.

Organ Batholith Zircon Crystallization Ages

Both Rioux et al. (2010) and this study dated zircons from the tuff of Squaw Mountain using TIMS. There is a 86 ka age difference between the weighted means of these two sets of data (36.253 ± 0.024 Ma vs. 36.167 ± 0.022 Ma, Rioux et al., 2010). The $^{206}Pb/^{238}U$ zircon ages of Rioux et al. (2010) were obtained at the Massachusetts Institute of Technology (MIT) Isotope Lab in Cambridge, Massachusetts, reduced using U-Pb Redux (McLean et al., 2011)

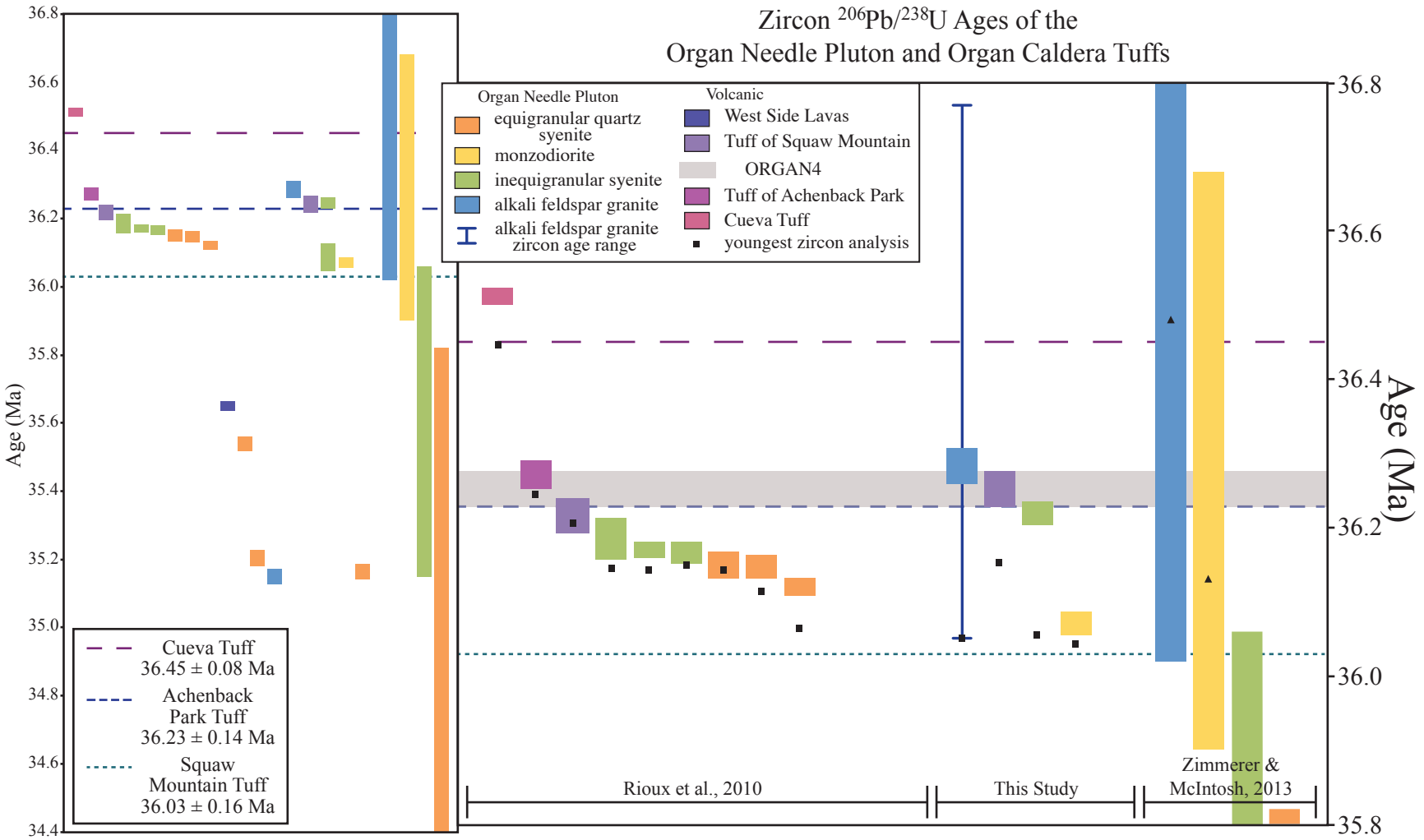

Figure 3. $^{206}Pb/^{238}U$ weighted mean ages for the compositional phases of the Organ Needle Pluton and for the three Organ Caldera ignimbrites. Each colored bar represents the weighted mean age and 2σ uncertainty of a single sample. Ages of Rioux et al. (2010) have been adjusted for laboratory bias (increased by 0.14%, ~50 ka). The grey bar is the weighted mean age of the tuff of Squaw Mountain (ORGAN4). Squares (▪) indicate youngest zircon analysis of individual TIMS samples. Triangles (▲) indicate weighted mean age of ICP-MS analyses. The dark blue line is the range of zircon ages for the alkali feldspar granite (ORGAN41). Dotted lines are $^{40}Ar/^{39}Ar$ eruption ages of the three ignimbrites from Zimmerer and McIntosh (2013).

and Th-corrected to a Th/U = 2.8. The difference in zircon ages due to the different Th/U values used by Rioux et al. (2010) and this study is ~30 ka (<0.1% of the zircon ages). Accounting for the Th-correction, the weighted mean zircon crystallization age of the tuff is still ~50 ka older than determined by Rioux et al. (2010). This suggests there is a laboratory bias between the UNC and MIT TIMS facilities, with UNC producing ages ~50 ka older (~0.1% of zircon ages) than those from MIT. This does not significantly affect the interpretations herein and ages have only been adjusted in Figures 3 and 6 (ages of Rioux et al., 2010, have been increased by 0.14%, ~50 ka).

Several observations should be noted from the combined data of Rioux et al. (2010) and this study. There are at least two distinct alkali feldspar granites within the Organ Needle Pluton (Figure 3). The alkali feldspar granite from this study (36.285 Ma) is more than 1 Ma older than the more northern alkali feldspar granite sampled by Rioux et al. (weighted mean age of 35.102 ± 0.022 Ma; 2010). Finally, as suggested above, samples of equigranular quartz syenite located closer in proximity to the alkali feldspar granite, inequigranular syenite and monzodiorite samples of this study are 36 Ma (Figure 3).

Implications for Current Petrogenetic Model

The geochemical model describing the construction of the Organ Needle Pluton developed by Verplanck et al., (1995; 1999) relies on fractional crystallization, crystal separation and magma migration to produce the chemical gradients observed across the individual compositional phases, as well as, the different compositional phases themselves. Chemical variation produced by differentiation of a single magma system in the upper crust by processes like fractional crystallization should have a specific pattern of zircon crystallization ages (Table 2). Silicic magma produced by differentiation from a more mafic

Table 2. Relative intrusion and commencement of cooling of the Organ Needle Pluton and eruption of the tuff of Squaw Mountain.

	Verplanck Model †	$^{206}Pb/^{238}U$ Ages ‡
youngest	Alkali Feldspar Granite/ Tuff of Squaw Mtn	Equigranular Qtz Syenite
	Inequigranular Syenite	Monzodiorite
	Monzodiorite	Inequigranular Syenite
oldest	Equigranular Qtz Syenite	Alkali Feldspar Granite/ Tuff of Squaw Mtn

† Age relations after the geochemical model of Verplanck et al., 1999.
‡ Age relations using the TIMS zircon ages from this study.

magma would be expected to have a younger crystallization history than its mafic counterpart since cooling and crystallization of the mafic magma leads to development of the silicic magmas (Hildreth, 1979; Tappa et al., 2011). Additionally, the ages of a complementary mafic magma should represent an extended crystallization history, reflecting the accumulation of sinking or residual crystals at lower magma depths over the lifetime of the system (Hildreth, 1981).

The age progression of the Organ Needle Pluton shows a change from silicic to more mafic chemistries over time, with the alkali feldspar granite preceding emplacement of the inequigranular syenite and monzodiorite (Figure 2, Table 2). The Organ Needle Pluton $^{206}Pb/^{238}U$ ages reflect the opposite of zircon crystallization ages expected from the differentiation of a single magma system (Table 2). The most silicic Organ Needle Pluton magmas have an older, extended zircon crystallization compared to the younger, discrete zircon ages of the monzodiorite (Figure 2). The tuff of Squaw Mountain and the alkali feldspar granite could not have been produced by fractional crystallization and crystal

separation/magma migration of the inequigranular syenite or the monzodiorite of the Organ Needle Pluton. Thus, the chemical variation observed in the Organ Needle Pluton did not originate by in-situ differentiation of a mafic magma in the upper crust.

Petrogenesis of the Organ Needle Pluton

Several geochemical models have been developed to describe the formation of high silica magmas, like the alkali feldspar granite and tuff of Squaw Mountain, within the upper crust (Hildreth, 1979; Hildreth, 1981; Kistler et al., 1986; Coleman and Walker, 1992; Bachmann et al., 2002; Bachmann and Bergantz, 2003). The two-fold fractional crystallization model of Verplanck et al. (1995, 1999) was developed after geochemical analysis excluded silicic magma production by pure melting of the Precambrian White Sands quartz monzonite or by simple mixing of a mafic magma with the local Precambrian wall rock (Butcher, 1990; Verplanck et al., 1995). Zircon crystallization geochronology excludes the possibility that the Organ Needle Pluton formed by fractional crystallization and crystal separation/magma migration (Table 2), however, other aspects of the geochemical model of Verplanck et al. (1995, 1999) are still relevant. Isotopic variation across the Organ Needle Pluton appears to be the result of assimilation of local Precambrian wall rock by a rising magma (Table 3).

The isotope geochemistry of the Organ Needle Pluton shows an overall change from heterogeneous radiogenic $^{87}Sr/^{86}Sr_i$ and low ε_{Nd} values to a uniform 0.7060 $^{87}Sr/^{86}Sr_i$ and -2 ε_{Nd} isotopic signature with time (Table 3). The chemical evolution of the Organ Needle Pluton appears to initially reflect variable assimilation of the White Sands pluton by a single -2 ε_{Nd} magma, which self buffers with continued magma injection and reflects a consistent, less evolved isotopic signature (Figures 4 and 5).

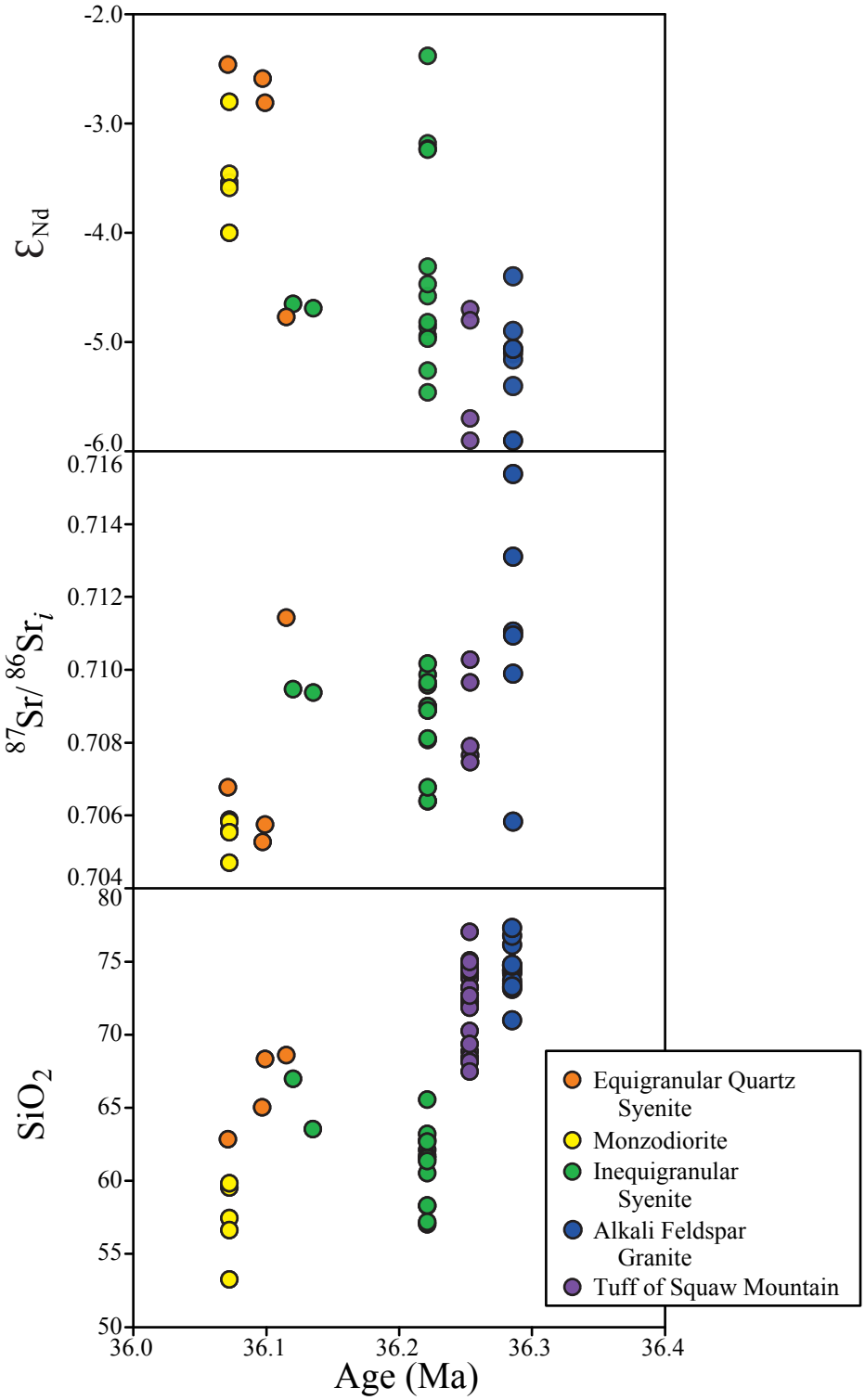

Figure 4. ε_{Nd}, $^{87}Sr/^{86}Sr_i$ and SiO_2 vs. zircon TIMS age for samples of the alkali feldspar granite, inequigranular syenite, monzodiorite, and equigranular quartz syenite phases of the Organ Needle Pluton and the tuff of Squaw Mountain. Ages are weighted mean zircon crystallization ages obtained in this study. Chemical analyses from Butcher (1990), Yanicak (1992), Verplanck et al. (1995, 1999). Verplanck et al. (1999) samples dated by Rioux et al. (2010) reflect their individual respective ages.

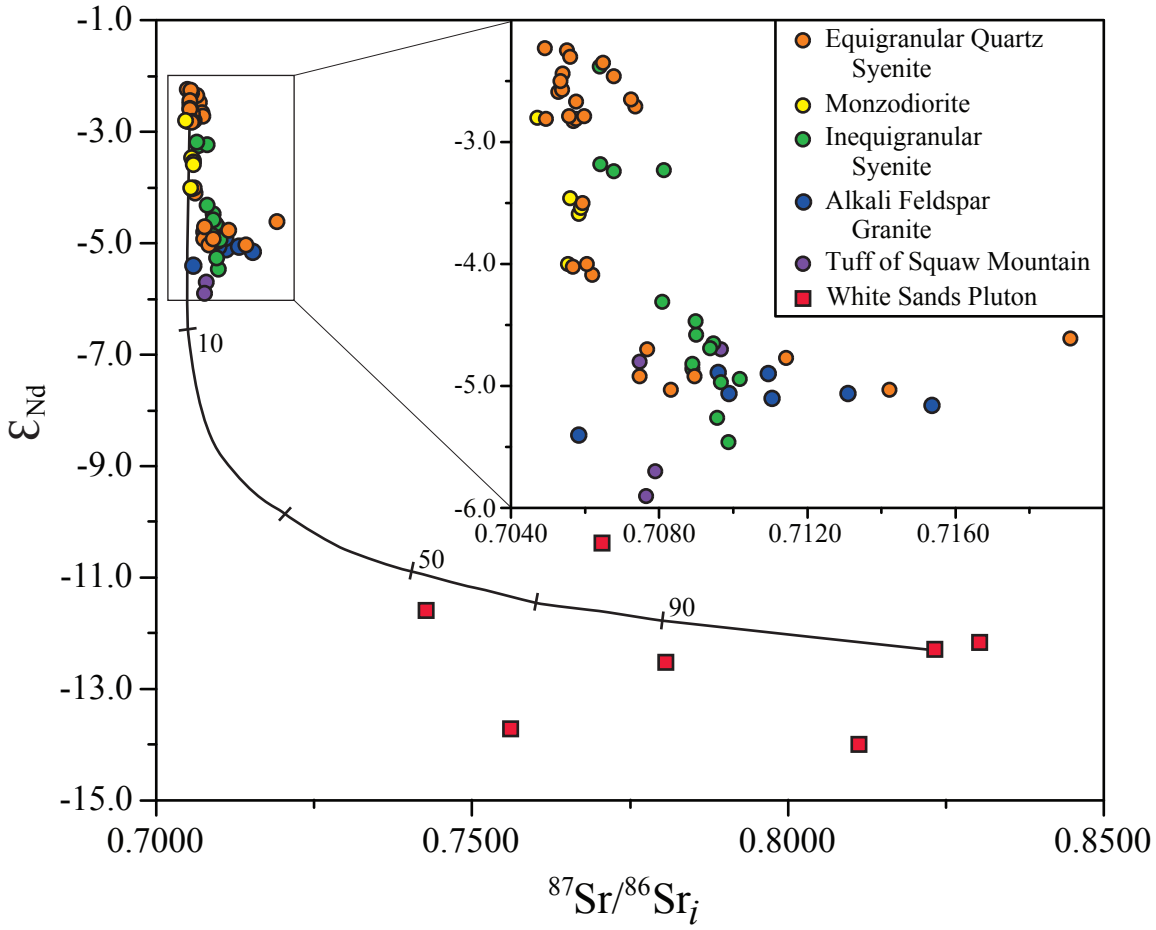

Figure 5. ε_{Nd} vs. $^{87}Sr/^{86}Sr_i$ for samples of the alkali feldspar granite, inequigranular syenite, monzodiorite, and equigranular quartz syenite phases of the Organ Needle Pluton and the tuff of Squaw Mountain. Colors reflect the zircon crystallization ages obtained in this study, with older ages in cool colors and younger ages in warm colors. Mixing line calculated after DePaolo and Wasserburg (1979) using Organ Needle Pluton equigranular quartz syenite sample 2701 and White Sands pluton sample 4291 as chemical endmembers (Verplanck et al., 1999). Tick marks denote weight fraction of Precambrian wall rock component at 20% intervals. Chemical analyses from Butcher (1990), Yanicak (1992), Verplanck et al. (1995, 1999).

Table 3. Isotopic variation of the Organ Needle Pluton and the tuff of Squaw Mountain.

		ε_{Nd}		$^{87}Sr/^{86}Sr_i$ *	
		Average	Range	Average	Range
youngest†	Equigranular Quartz Syenite	-2	-2.3 to -2.8	0.7060	0.7054-0.7056
	Monzodiorite	-3.5	-3.5 to -3.6	0.706	0.7056-0.7059
	Inequigranular Syenite	<-4.5	-3.2 to -5.5	~0.7085	0.7075-0.7191
	Alkali Feldspar Granite	-5	-4.9 to -5.2	>0.709	0.7099-0.7153
	Tuff of Squaw Mountain ‡	-5	-4.7 to -5.9	~0.709	0.7075-0.7103
oldest	White Sands Quartz Monzonite	-12.1	-10.4 to -13.7	0.784 §	0.7427-0.8303 §

* All isotope data, except for tuff of Squaw Mountain from Verplanck et al., 1995 and 1999.
† Age relations after ID-TIMS zircon ages from this study.
‡ Isotope data for tuff of Squaw Mountain from Butcher, 1990.
§ $^{87}Sr/^{86}Sr$ at 36 Ma.

The compositional zonation and chemical heterogeneity of the system could indicate varied assimilation across a large magma body, with individual SiO_2 compositions reflecting the amount of assimilate. However, if the major element chemistry were dictated by the degree of assimilation, the most mafic chemistries would also be isotopically the least radiogenic (Figures 4 and 5, Table 3). For the Organ Needle Pluton, the monzodiorite has lower ε_{Nd} values than those of the equigranular quartz syenite. The compositional zonation exhibited by the pluton is likely produced by chemically distinct magmas that evolved by lower crustal processes (Coleman et al., 2004; Glazner et al., 2004; Clemens et al., 2010; Tappa et al., 2011).

A straightforward model of incremental emplacement of differentiated, -2 ε_{Nd} magmas with decreasing Precambrian basement assimilation over time describes the field

observations, the whole rock and isotope geochemistry, and zircon crystallization ages of the Organ Needle Pluton. The magma chemistry of individual magma batches appears to have been inherited from evolution at lower crustal levels, whereas isotopic chemistry reflects the amount of assimilated local basement within each batch. Initial magma injection beneath the Organ Mountains assimilated small amounts of the local basement, suggested by the more radiogenic isotopic signature of the oldest Organ Needle Pluton phases, alkali feldspar granite and inequigranular syenite, and the pervasive presence of Precambrian xenoliths within the inequigranular syenite (Figure 4; Seager, 1981; Verplanck et al., 1995, 1999). With time, the Precambrian basement contributed less material to the rising magma as it became locally unavailable due to replacement by Organ Needle Pluton magmas or less significant as magma flux increased. Given the general lack of Precambrian xenoliths within the equigranular quartz syenite, the former scenario is preferred (Seager, 1981; Verplanck et al., 1995, 1999).

Implications for Ignimbrite-Pluton Relationships

The $^{206}Pb/^{238}U$ weighted mean ages for the alkali feldspar granite and the tuff of Squaw Mountain overlap within uncertainty (Figure 6), which does not preclude their possible genetic affiliation (Butcher et al., 1989; Verplanck et al., 1995). The alkali feldspar granite has a greater range of zircon ages than the more constrained zircon age range of the tuff (Figures 2 and 3). In fact, the alkali feldspar granite zircon crystallization ages (36.77 to 36.05 Ma) span the $^{206}Pb/^{238}U$ zircon ages of all three ignimbrites (weighted mean ages of 36.462 ± 0.012 Ma, Cueva tuff and 36.222 ± 0.019 Ma, tuff of Achenback Peak, Rioux et al., 2010; 36.253 ± 0.024 Ma, tuff of Squaw Mountain, this study; Figures 3 and 6). This may indicate extended emplacement of the alkali feldspar granite magma prior to injection and

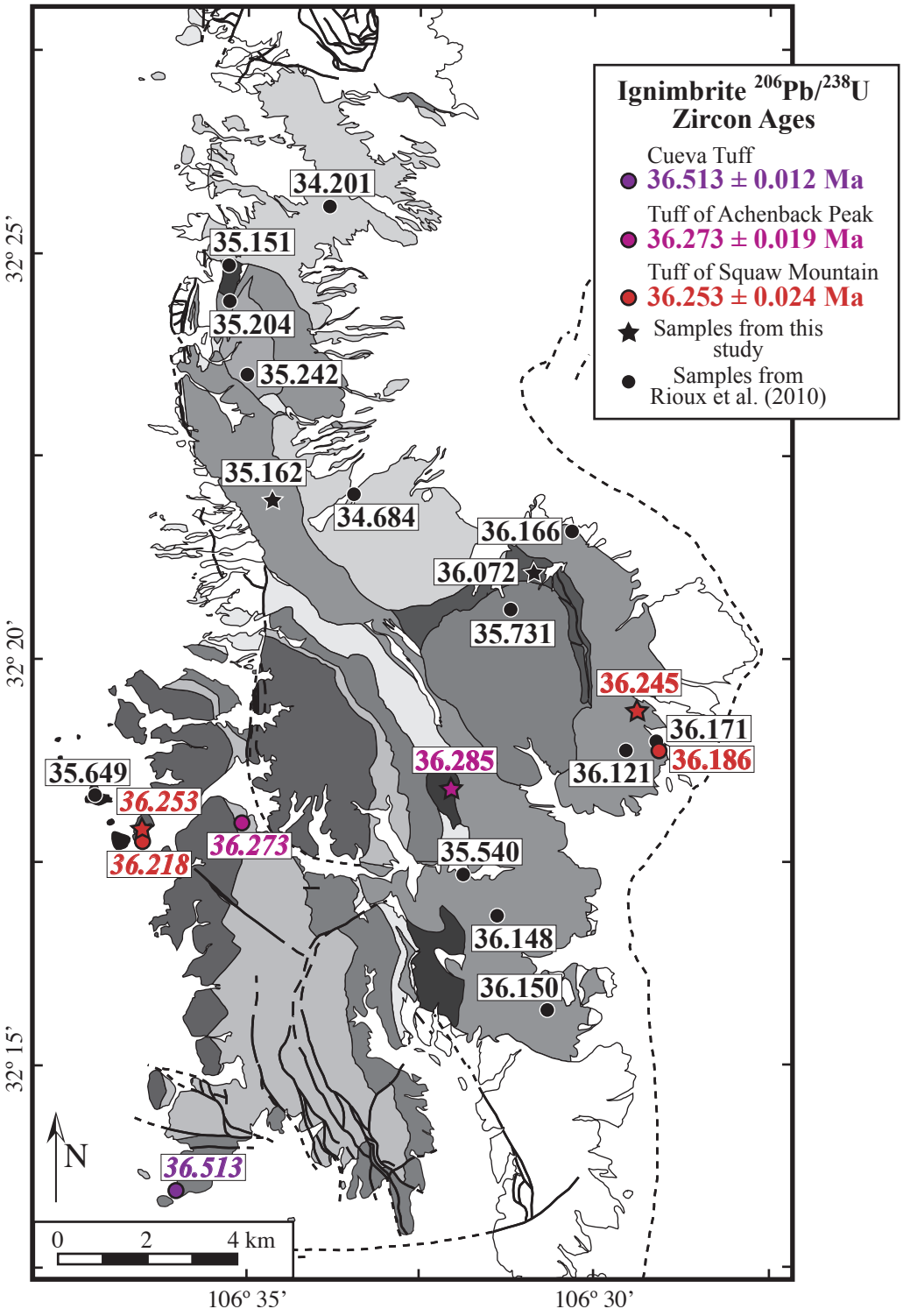

Figure 6. Geographic distribution of $^{206}Pb/^{238}U$ zircon crystallization ages within uncertainty of the weighted mean ages of the three Organ Caldera ignimbrites (italicized). Sample names are given in Figure 1. Ages are $^{206}Pb/^{238}U$ weighted mean ages from this study and Rioux et al. (2010). Ages of Rioux et al. (2010) have been adjusted for laboratory bias (increased by 0.14%, ~50 ka). Geologic map of the Organ Mountains after Seager (1981) and Verplanck et al. (1999).

eruption of the tuff magma. This would allow for each being a separate and distinct magma or for the tuff magma to represent continued injection of the alkali feldspar granite magma into the region. If they do represent the same magma however, perhaps an increase in magma flux allowed for the change from emplacement to eruption (Mills and Coleman, 2013; Schöpa and Annen, 2013). Given the chemical, isotopic and spatiotemporal comparisons, it is possible that the central exposure of alkali feldspar granite represents unerupted remnants of the tuff of Squaw Mountain (Figure 1).

The $^{206}Pb/^{238}U$ weighted mean age of the oldest zircon population of the inequigranular syenite is identical to the weighted mean age of the tuff of Squaw Mountain (Figure 2). Additionally, the younger zircon population of the inequigranular syenite is statistically identical to the $^{206}Pb/^{238}U$ zircon weighted mean age of the monzodiorite (Figure 2). The inequigranular syenite could have inherited zircons from the tuff of Squaw Mountain, but have been emplaced and cooled at the same time as the monzodiorite.

The zircon ages of the alkali feldspar granite and the inequigranular syenite of this study and one sample of inequigranular syenite (PV5292, adjusted age) of Rioux et al. (2010) are the only Organ Needle Pluton zircon analyses that overlap with the zircon ages of the Organ Caldera ignimbrites (Figure 6). The great majority of the Organ Needle Pluton appears to be a separate, younger magmatic event from the older ignimbrites. The range in zircon ages for the alkali feldspar granite allows for the possibility that it is related to the tuff of Squaw Mountain, however, the preferred age for the alkali feldspar granite is the weighted mean age, which is older than the tuff.

Organ Needle Pluton Magma Flux

The Organ Batholith is exposed over about 100 km^2, and about half of that exposure has been mapped as the Organ Needle Pluton (Seager, 1981; Verplanck et al., 1995, 1999). From west to east, the longest exposure of the Organ Needle Pluton is about 6 km, and the region has been tilted 15-20° since pluton emplacement (Seager, 1981; Seager and McCurry, 1988). This results is an exposed paleodepth of ~2 km and a minimum volume of ~100 km^3 for the Organ Needle Pluton.

The weighted mean ages and the youngest zircon crystallization ages give nearly identical age ranges between the oldest Organ Needle Pluton phase, the alkali feldspar granite and the youngest phase, the equigranular quartz syenite – 1.123 Ma (36.285 Ma and 35.162 Ma weighted mean ages) and 1.133 Ma (36.052 Ma and 34.919 Ma youngest zircon age), respectively. This is a minimum age range, as continued geochronologic analysis would increase or maintain this range. The magma flux for the Organ Needle Pluton using either age range is 0.00009 km^3/a.

Thermal History of the Organ Needle Pluton

Several important age relationships and patterns are noticeable with the combination of the geochronology of Rioux et al. (2010), Zimmerer and McIntosh (2013), and this study (Figure 3), and assessing the Organ Batholith as a whole (Figures 7 and 8). $^{206}Pb/^{238}U$ zircon ages across the entire Organ Mountains indicate the Organ Batholith was incrementally emplaced over almost 3 Ma (Figure 7). Emplacement began in the southern mountains around 36.7 Ma (alkali feldspar granite from this study) and progressed north, where emplacement ages average closer to 35.0 Ma (alkali feldspar granite PV3491 of Rioux et al., 2010). A south to north spatiotemporal trend is also observable for the $^{40}Ar/^{39}Ar$ biotite

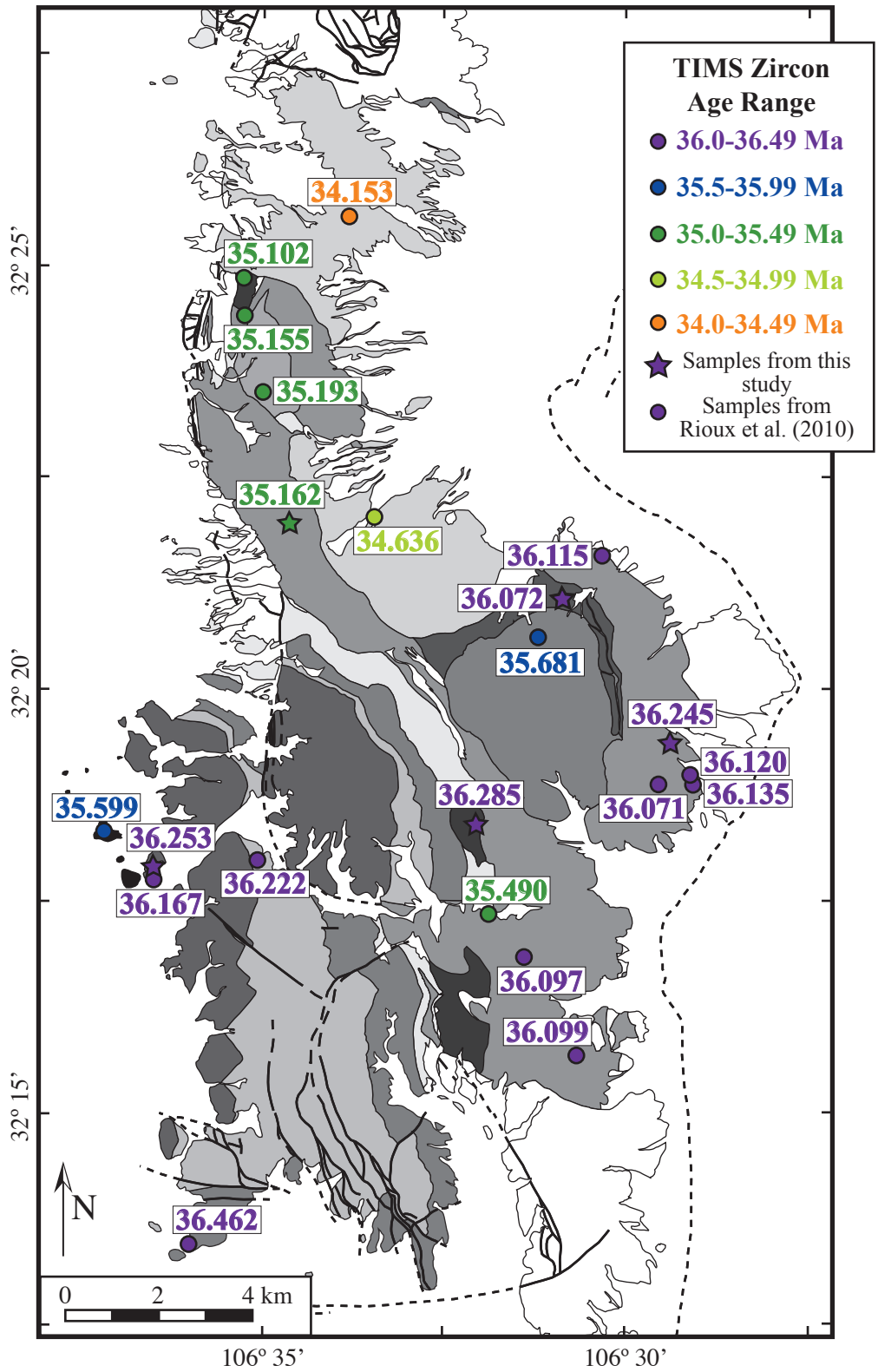

Figure 7. Geographic distribution of $^{206}Pb/^{238}U$ zircon TIMS ages. Sample names are given in Figure 1 and ages are $^{206}Pb/^{238}U$ weighted mean ages from this study and Rioux et al. (2010). No ages have been adjusted for laboratory bias. Geologic map of the Organ Mountains after Seager (1981) and Verplanck et al. (1999).

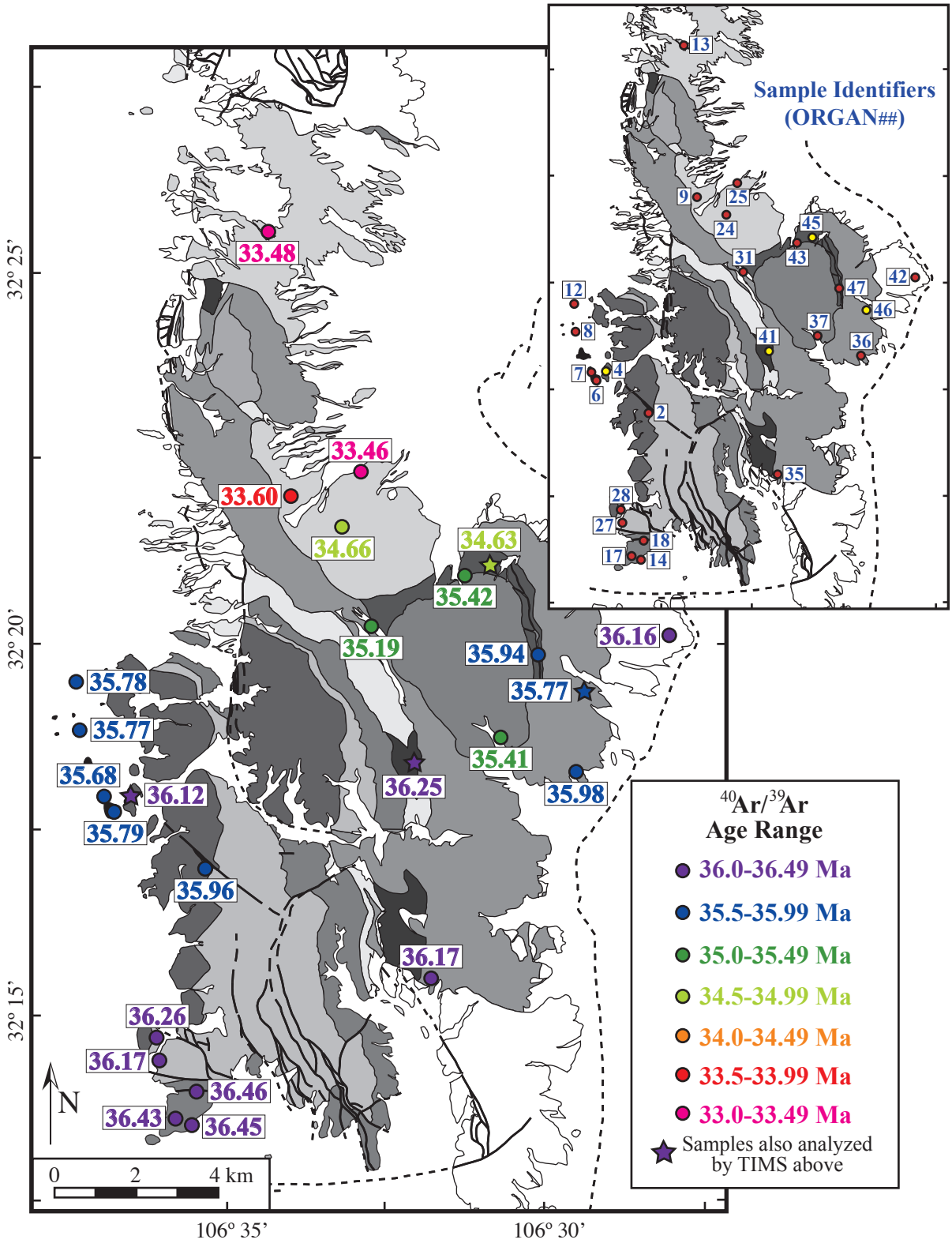

Figure 8. Geographic distribution of $^{40}Ar/^{39}Ar$ biotite cooling ages. Sample locations are shown in the inset map. Ages are $^{40}Ar/^{39}Ar$ sanidine eruption and biotite cooling ages from Zimmerer and McIntosh (2013). Geologic map of the Organ Mountains after Seager (1981) and Verplanck et al. (1999).

cooling ages of Zimmerer and McIntosh (2013; Figure 8). The top-down crystallization and cooling of a pluton could produce a similar trend if the structural top of the Organ Needle Pluton were in the southern Organ Mountains (the oldest zircon and biotite ages) and paleodepth increased to the north. However, the Organ Needle Pluton and surrounding rocks have been tilted nearly directly westward and paleodepth increases from west to east, so the cooling trend must reflect changes in magma emplacement with time (Figure 1; Seager, 1981). Emplacement of magma into the upper crust moved north over ~1 Ma and, as noted by Zimmerer and McIntosh (2013) was followed by fast cooling across the batholith.

Conclusion

New, high-precision $^{206}Pb/^{238}U$ zircon ages from the Organ Needle Pluton support formation of the compositionally zoned pluton by incremental emplacement of small, isotopically uniform, compositionally distinct magma batches that individually assimilated varying amounts of local Precambrian quartz monzonite. Significantly, intrusion into the shallow crust began with an alkali feldspar granite at 36.285 ± 0.024 Ma, and continued with successive emplacement of increasingly more mafic magmas – an inequigranular syenite at 36.221 ± 0.016 Ma, and then a monzodiorite at 36.072 ± 0.016 Ma. The zircon crystallization ages of these three phases of the Organ Needle Pluton support recent proposals that magma chemistry is an artifact of source evolution and preclude the possibility that the zoned chemistry of the Organ Needle Pluton resulted from differentiation of the monzodiorite or another mafic magma in-situ (Tappa et al., 2011; Coleman et al., 2012).

The zircon ages for the tuff of Squaw Mountain and the alkali feldspar granite of the Organ Needle Pluton overlap and support the possibility that the Organ Needle Pluton alkali feldspar granite as the unerupted equivalent of the tuff of Squaw Mountain (Butcher et al.,

1989; Verplanck et al., 1995; Zimmerer and McIntosh, 2013). However, the majority of Organ Needle Pluton was emplaced with no interaction with the Organ Caldera ignimbrites, and the eruption of the ignimbrites appears to be an older, separate magmatic event from emplacement of the pluton.

The equigranular quartz syenite zircons analyzed in this study are ~1 Ma younger than the other Organ Needle Pluton phases and agree with the preliminary ages reported by Zimmerer and McIntosh (2013). Samples of equigranular quartz syenite located closer to the three other Organ Needle Pluton samples have zircon crystallization ages of 36 Ma (Rioux et al., 2010).

Finally, the Organ Batholith was emplaced between 36.77 Ma and 34.3 Ma. Both $^{206}Pb/^{238}U$ zircon crystallization ages and $^{40}Ar/^{39}Ar$ biotite cooling ages indicate emplacement and cooling of the Organ Batholith began in the south and migrated to the north over time (Zimmerer and McIntosh, 2013).

APPENDIX

Sample	Composition			Isotopic Ratios							Dates (Ma) [a]				
Fraction (n)	U (ppm)	Pb* (pg) [b]	Th/U [c]	$^{206}Pb/^{204}Pb$ [d]	$^{206}Pb/^{238}U$ [e]	±2σ %	$^{207}Pb/^{235}U$ [e]	±2σ %	$^{207}Pb/^{206}Pb$	±2σ %	$^{206}Pb/^{238}U$ [f]	±2σ abs	$^{207}Pb/^{235}U$	$^{207}Pb/^{206}Pb$	Pbc (pg) [g]
ORGAN4 Tuff of Squaw Mountain (Th/U = 4.7; 0348650 3574050) [h]															
3 (2)	514	47.9	2.720	418.4	0.005639	(.11)	0.03669	(0.9)	0.04719	(0.9)	36.29	.04	36.58	58.7	4.6
5 (3)	318	27.0	2.208	196.9	0.005615	(.17)	0.03599	(1.9)	0.04649	(1.8)	36.16	.06	35.90	22.9	6.4
6 (3)	190	14.9	1.757	85.5	0.005624	(.24)	0.03800	(3.9)	0.04901	(3.7)	36.22	.09	37.87	148.2	10.2
7 (4)	273	20.9	1.651	359.5	0.005630	(.12)	0.03669	(1.1)	0.04727	(1.0)	36.26	.04	36.59	62.8	2.9
10 (2)	192	31.2	1.959	424.9	0.005631	(.17)	0.03564	(1.6)	0.04590	(1.5)	36.26	.06	35.56	-7.4	3.4
ORGAN10 Equigranular Quartz Syenite (Th/U = 4.7; 0351675 3581925)															
1 (1)	84	8.7	1.049	168.8	0.005435	(.23)	0.03559	(2.6)	0.04749	(2.4)	35.03	.08	35.51	74.1	3.1
2 (1)	107	17.3	1.408	294.1	0.005462	(.19)	0.03597	(1.8)	0.04776	(1.7)	35.19	.07	35.88	87.3	3.1
4 (3)	108	23.9	1.186	302.2	0.005440	(.14)	0.03579	(1.1)	0.04772	(1.1)	35.05	.05	35.70	85.2	4.4
5 (2)	165	17.7	1.203	552.9	0.005419	(.26)	0.03571	(1.3)	0.04780	(1.2)	34.92	.09	35.63	89.4	1.7
8 (2)	187	25.3	1.217	177.9	0.005462	(.16)	0.03624	(1.8)	0.04813	(1.7)	35.19	.06	36.15	105.5	8.2
10 (1)	85	10.0	1.272	111.7	0.005493	(.34)	0.03535	(4.9)	0.04667	(4.6)	35.39	.12	35.27	32.6	5.5
11 (2)	146	13.7	1.146	167.6	0.005473	(.28)	0.03553	(4.1)	0.04709	(3.9)	35.26	.10	35.45	53.7	4.8
12 (2)	227	11.2	1.404	179.2	0.005475	(.18)	0.03554	(2.1)	0.04709	(2.0)	35.27	.06	35.47	53.6	3.5
14 (2)	85	8.5	1.457	322.6	0.005460	(.20)	0.03487	(1.4)	0.04632	(1.3)	35.17	.07	34.81	14.5	1.4
15 (2)	131	8.9	1.237	92.2	0.005493	(.48)	0.03395	(6.7)	0.04483	(6.3)	35.39	.17	33.90	-64.8	6.2
18 (1)	0	6.4	1.596	76.5	0.005488	(.31)	0.03632	(4.5)	0.04799	(4.3)	35.35	.11	36.22	99.0	5.3

[a] Isotopic dates calculated using the decay constants $\lambda_{238} = 1.55125E^{-10}$ and $\lambda_{235} = 9.8485E^{-10}$ (Jaffey et al., 1971).
[b] Total mass of radiogenic Pb.
[c] Th composition calculated from radiogenic ^{208}Pb and the $^{207}Pb/^{206}Pb$ date of the sample, assuming concordance between U-Th and Pb systems.
[d] Measured ratio corrected for fractionation and spike contribution only.
[e] Measured ratios corrected for fractionation, tracer and blank.
[f] Corrected for initial Th/U disequilibrium using radiogenic ^{208}Pb and average Th/U calculated from geochemical analyses of Butcher, 1990, and Verplanck and others, 1999.
[g] Total mass of common Pb.
[h] Sample locations are listed as UTM coordinates in Section 13S, NAD 27 (Zimmerer and McIntosh, 2013).

Sample	Composition			Isotopic Ratios							Dates (Ma) [a]				
Fraction (n)	U (ppm)	Pb* (pg) [b]	Th/U [c]	$^{206}Pb/^{204}Pb$ [d]	$^{206}Pb/^{238}U$ [e]	±2σ %	$^{207}Pb/^{235}U$ [e]	±2σ %	$^{207}Pb/^{206}Pb$	±2σ %	$^{206}Pb/^{238}U$ [f]	±2σ abs	$^{207}Pb/^{235}U$	$^{207}Pb/^{206}Pb$	Pbc (pg) [g]
ORGAN41 Alkali Feldspar Granite (Th/U = 6.6; 0355614 3574574)															
1 (1)	404	51.6	2.199	888.4	0.005631	(.13)	0.03655	(0.5)	0.04707	(0.5)	36.27	.05	36.45	52.6	2.5
2 (1)	385	13.0	1.116	212.1	0.005594	(.17)	0.03646	(1.8)	0.04727	(1.7)	36.05	.06	36.36	62.8	3.5
3 (2)	226	6.3	1.216	246.7	0.005612	(.25)	0.03641	(2.7)	0.04706	(2.5)	36.16	.09	36.31	52.1	1.4
7 (3)	269	13.6	1.358	288.1	0.005675	(.37)	0.03785	(4.2)	0.04837	(4.0)	36.57	.13	37.72	117.6	2.5
8 (3)	260	25.2	1.509	706.8	0.005644	(.35)	0.03682	(1.5)	0.04732	(1.4)	36.36	.13	36.72	65.3	1.8
10 (1)	890	7.0	1.764	96.1	0.005634	(.29)	0.03496	(4.5)	0.04501	(4.3)	36.30	.10	34.90	-55.0	4.1
13 (1)	76	5.8	1.582	66.1	0.005707	(.46)	0.03809	(6.6)	0.04840	(6.2)	36.77	.17	37.95	118.7	5.9
14 (2)	96	6.3	1.440	125.0	0.005651	(.20)	0.03772	(2.8)	0.04841	(2.6)	36.41	.07	37.60	119.6	2.9
15 (2)	177	4.1	1.637	95.6	0.005653	(.29)	0.03667	(4.2)	0.04705	(4.0)	36.42	.10	36.57	51.6	2.5
16 (3)	442	12.8	1.397	211.8	0.005635	(.15)	0.03643	(1.8)	0.04688	(1.7)	36.31	.05	36.33	43.3	3.3
ORGAN45 Monzodiorite (Th/U = 5.9; 0360051 3577609)															
1 (1)	519	77.0	0.902	1674.4	0.005604	(.10)	0.03619	(0.3)	0.04684	(0.2)	36.11	.04	36.10	40.9	2.6
2 (1)	865	92.9	1.078	2798.2	0.005594	(.10)	0.03603	(0.3)	0.04672	(0.2)	36.05	.03	35.95	34.8	1.8
3 (2)	627	46.0	1.053	684.9	0.005598	(.16)	0.03604	(0.9)	0.04669	(0.9)	36.08	.06	35.95	33.5	3.7
4 (2)	387	48.4	1.227	641.4	0.005594	(.11)	0.03626	(0.6)	0.04701	(0.5)	36.04	.04	36.16	49.8	4.0
5 (1)	466	29.1	0.767	259.2	0.005605	(.20)	0.03682	(1.7)	0.04765	(1.6)	36.12	.07	36.72	82.0	6.9
6 (1)	411	36.3	0.809	870.6	0.005595	(.10)	0.03645	(0.5)	0.04725	(0.4)	36.06	.04	36.35	61.7	2.4
8 (1)	709	49.2	1.222	186.3	0.005600	(.17)	0.03632	(1.9)	0.04704	(1.8)	36.09	.06	36.23	51.5	15.1

[a] Isotopic dates calculated using the decay constants $\lambda_{238} = 1.55125E^{-10}$ and $\lambda_{235} = 9.8485E^{-10}$ (Jaffey et al., 1971).
[b] Total mass of radiogenic Pb.
[c] Th composition calculated from radiogenic ^{208}Pb and the $^{207}Pb/^{206}Pb$ date of the sample, assuming concordance between U-Th and Pb systems.
[d] Measured ratio corrected for fractionation and spike contribution only.
[e] Measured ratios corrected for fractionation, tracer and blank.
[f] Corrected for initial Th/U disequilibrium using radiogenic ^{208}Pb and average Th/U calculated from geochemical analyses of Butcher, 1990, and Verplanck and others, 1999.
[g] Total mass of common Pb.
[h] Sample locations are listed as UTM coordinates in Section 13S, NAD 27 (Zimmerer and McIntosh, 2013).

Sample	Composition			Isotopic Ratios							Dates (Ma) [a]				
Fraction (n)	U (ppm)	Pb* (pg) [b]	Th/U [c]	$^{206}Pb/^{204}Pb$ [d]	$^{206}Pb/^{238}U$ [e]	±2σ %	$^{207}Pb/^{235}U$ [e]	±2σ %	$^{207}Pb/^{206}Pb$	±2σ %	$^{206}Pb/^{238}U$ [f]	±2σ abs	$^{207}Pb/^{235}U$	$^{207}Pb/^{206}Pb$	Pbc (pg) [g]
ORGAN46 Inequigranular Syenite (Th/U = 3.9; 0356294 3580066)															
1 (1)	177	75.6	1.485	1641.6	0.005604	(.13)	0.03617	(0.4)	0.04681	(0.4)	36.09	.05	36.07	39.3	2.3
2 (1)	169	100.1	1.404	2807.0	0.005598	(.25)	0.03630	(0.4)	0.04703	(0.3)	36.05	.09	36.20	50.8	1.8
3 (2)	167	90.5	1.158	1161.5	0.005627	(.10)	0.03666	(0.3)	0.04725	(0.3)	36.25	.04	36.55	61.9	4.1
4 (2)	168	68.6	1.595	1015.8	0.005622	(.09)	0.03656	(0.4)	0.04716	(0.4)	36.21	.03	36.46	57.5	3.3
6 (1)	180	120.2	0.761	2308.8	0.005625	(.08)	0.03621	(0.2)	0.04669	(0.2)	36.25	.03	36.12	33.6	3.0
7 (1)	114	48.6	1.531	547.1	0.005635	(.11)	0.03663	(0.7)	0.04714	(0.6)	36.29	.04	36.53	56.4	4.4
8 (1)	165	126.7	0.861	253.7	0.005629	(.22)	0.03641	(2.1)	0.04691	(2.0)	36.27	.08	36.31	44.5	30.2

[a] Isotopic dates calculated using the decay constants $\lambda_{238} = 1.55125E^{-10}$ and $\lambda_{235} = 9.8485E^{-10}$ (Jaffey et al., 1971).
[b] Total mass of radiogenic Pb.
[c] Th composition calculated from radiogenic ^{208}Pb and the $^{207}Pb/^{206}Pb$ date of the sample, assuming concordance between U-Th and Pb systems.
[d] Measured ratio corrected for fractionation and spike contribution only.
[e] Measured ratios corrected for fractionation, tracer and blank.
[f] Corrected for initial Th/U disequilibrium using radiogenic ^{208}Pb and average Th/U calculated from geochemical analyses of Butcher, 1990, and Verplanck and others, 1999.
[g] Total mass of common Pb.
[h] Sample locations are listed as UTM coordinates in Section 13S, NAD 27 (Zimmerer and McIntosh, 2013).

REFERENCES

Agostinetti, N.P., and Chiarabba, C., 2008, Seismic structure beneath Mt Vesuvius from receiver function analysis and local earthquakes tomography: Evidences for location and geometry of the magma chamber: Geophysical Journal International, v. 175, p. 1298-1308.

Annen, C., 2009, From plutons to magma chambers: Thermal constraints on the accumulation of eruptible silicic magma in the upper crust: Earth and Planetary Science Letters, v. 284, p. 409-416.

Bachmann, O., and Bergantz, G.W., 2003, Rejuvenation of the Fish Canyon magma body: A window into the evolution of large-volume silicic magma systems: Geology, v. 31, p. 789-792.

Bachmann, O., Charlier, B.L.A., and Lowenstern, J.B., 2007, Zircon crystallization and recycling in the magma chamber of the rhyolitic Kos Plateau Tuff (Aegean arc): Geology, v. 35, p. 73-76.

Bachmann, O., Dungan, M.A., and Lipman, P.W., 2002, Fish Canyon Magma Body, San Juan Volcanic Field, Colorado: Rejuvenation and eruption of an upper-crustal batholith: Journal of Petrology, v. 43, p. 1469-1503.

Bateman, P.C., and Chappell, B.W., 1979, Crystallization, fractionation, and solidification of the Tuolumne intrusive series, Yosemite National Park, California: Geological Society of America Bulletin, v. 90, p. 465-482.

Beard, J.S., Ragland, P.C., and Crawford, M.L., 2005, Reactive bulk assimilation: A model for crust-mantle mixing in silicic magmas: Geology, v. 33, p. 681-684.

Butcher, D.P., 1990, Geochemistry and Nd/Sr systematics of selected lithologic units of the Oligocene Organ Cauldron and Batholith, south central New Mexico [M.S. thesis]: Las Cruces, New Mexico State University, 145 pp.

Butcher, D.P., McCurry, M., and Farmer, G.L., 1989, Evolution of the early Oligocene Organ Cauldron, South Central New Mexico [abs.]: New Mexico Bureau of Mines and Mineral Resources Bulletin, v. 131, p. 35.

Chapin, C.E., Wilks, M., and McIntosh, W.C., 2004, Space-time patterns of Late Cretaceous to present magmatism in New Mexico – comparison with Andean volcanism and potential for future volcanism: New Mexico Bureau of Geology and Mineral Resources, Bulletin, v. 160, p. 13-40.

Charlier, B.L.A., Wilson, C.J.N., Lowenstern, J.B., Blake, S., Van Calsteren, P.W., and Davidson, J.P., 2005, Magma generation at a large hyperactive silicic volcano (Taupo, New Zealand) revealed by U-Th and U-Pb systematics in zircons: Journal of Petrology, v. 46, p. 3-32.

Clemens, J.D., Helps, P.A., and Stevens, G., 2010, Chemical structure in granitic magmas – a signal from the source?: Earth and Environmental Science Transactions of the Royal Society of Edinburgh, v. 100, p. 159-172.

Coleman, D.S., and Walker, J.D., 1992, Evidence for the generation of juvenile granitic crust during continental extension, Mineral Mountains batholith, Utah: Journal of Geophysical Research: Solid Earth, v. 97, p. 11011-11024.

Coleman, D.S., Bartley, J.M., Glazner, A.F., and Pardue, M.J., 2012, Is chemical zonation in plutonic rocks driven by changes in source magma composition or shallow-crustal differentiation?: Geosphere, v. 8, p. 1568-1587.

Coleman, D.S., Gray, W., and Glazner, A.F., 2004, Rethinking the emplacement and evolution of zoned plutons: Geochronologic evidence for incremental assembly of the Tuolumne Intrusive Suite, California: Geology, v. 32, p.433-436.

Condie, K.C. and Budding, A.J., 1979, Geology and geochemistry of Precambrian rocks, central and south-central New Mexico: New Mexico Bureau of Mines and Mineral Resources Memoir 35, 58 p.

Davis, J.W., Coleman, D.S., Gracely, J.T., Gaschnig, R., and Stearns, M., 2012, Magma accumulation rates and thermal histories of plutons of the Sierra Nevada batholith, CA: Contributions to Mineralogy and Petrology: v. 163, p. 449-465.

DePaolo, D.J., and Wasserburg, G.J., 1979, Petrogenetic mixing models and Nd-Sr isotopic patterns: Geochimica et Cosmochimica Acta, v. 43, p. 615-627.

Dunham, K.C., 1935, The geology of the Organ Mountains: New Mexico Bureau of Mines and Mineral Resources Bulletin, v. 11, 272 p.

Glazner, A.F., Bartley, J.M., Coleman, D.S., Gray, W., and Taylor, R.Z., 2004, Are plutons assembled over millions of years by amalgamation from small magma chambers?: GSA Today, v. 14, p. 4-11.

Harrison, T.M., Duncan, I., and McDougall, I., 1985, Diffusion of ^{40}Ar in biotite: temperature, pressure and compositional effects: Geochimica et Cosmochimica Acta, v. 49, p. 2461-2468.

Harrison, T.M., Watson, E.B., and Aikman, A.B., 2007, Temperature spectra of zircon crystallization in plutonic rocks: Geology, v. 35, p. 635-638.

Hildreth, W., 1979, The Bishop Tuff: Evidence for the origin of compositional zonation in silicic magma chambers: Geological Society of America Special Paper 180, p. 43-75.

Hildreth, W., 1981, Gradients in silicic magma chambers: Implications for lithospheric magmatism: Journal of Geophysical Research, v. 86, p. 10153-10192.

Hildreth, W., and Wilson, C.J.N., 2007, Compositional zoning of the Bishop Tuff: Journal of Petrology, v. 48, p. 951-999.

Hirt, W. H., 2007, Petrology of the Mount Whitney Intrusive Suite, eastern Sierra Nevada, California: implications for the emplacement and differentiation of composite felsic intrusions: Geological Society of America Bulletin, v. 119, p. 1185-1200.

Iyer, H.M., 1979, Deep structure under Yellowstone National Park, U.S.A.: a continental "hot spot": Tectonophysics, v. 56, p. 165-197.

Jaffey, A.H., Flynn, K.F., Glendenin, L.E., Bently, W.C., and Essling, A.M., 1971, Precision measurement of the half-lives and specific activities of U235 and U238, Physical Review C, v. 4, p. 1889-1906.

Kistler, R.W., Chappell, B.W., Peck, D.L., and Bateman, P.C., 1986, Isotopic variation in the Tuolumne intrusive suite, central Sierra Nevada, California: Contributions to Mineralogy and Petrology, v. 94, p. 205-220.

Lees, J.M., 1992, The magma system of Mount St. Helens: Non-linear high-resolution P-wave tomography: Journal of Volcanology and Geothermal Research, v. 53, p. 103-116.

Lees, J.M., 2007, Seismic tomography of magmatic systems: Journal of Volcanology and Geothermal Research, v. 167, p. 37-56.

Lees, J.M., Symons, N., Chubarova, O., Gorelchik, V., and Ozerov, A., 2007, Tomographic images of Klyuchevskoy Volcano P-wave velocity: Volcanism and Subduction: The Kamchatka Region: American Geophysical Union Geophysical Monograph Series 172, p. 293-302.

Lipman, P.W., 1984, The roots of ash flow calderas in western North America: windows into the tops of granitic batholiths: Journal of Geophysical Research, v. 89, p. 8801-8841.

Lipman, P.W., 2007, Incremental assembly and prolonged consolidation of Cordilleran magma chambers: Evidence from the Southern Rocky Mountain volcanic field: Geosphere, v. 3, p. 42-70.

Lipman, P.W., Christiansen, R.L., and O'Connor, J.T., 1966, A compositionally zoned ash-flow sheet in Southern Nevada: Geological Survey Professional Paper 524-F, 47 p.

Masturyono, McCaffrey, R., Wark, D.A., Roecker, S.W., Ibrahim, F., Ibrahim, G., and Sukhyar, 2001, Distribution of magma beneath the Toba caldera complex, north Sumatra, Indonesia, constrained by three-dimensional P wave velocities, seismicity, and gravity data: Geochemistry, Geophysics, Geosystems, v. 2, 24 p.

Mahon, K.I., 1996, The New "York" regression: Application of an improved statistical method to geochemistry: International Geology Review, v. 38, p. 293-303.

Mattinson, J.M., 1973, Anomalous isotopic composition of lead in young zircons: Carnegie Institution of Washington Yearbook, v. 72, p. 613-616.

Mattinson, J.M., 2005, Zircon U-Pb chemical abrasion ("CA-TIMS") method: Combined annealing and multi-step partial dissolution analysis for improved precision and accuracy of zircon ages: Chemical Geology, v. 220, p. 47-66.

McDougall, I., and Harrison, T.M., 1999, Geochronology and Thermochronology by the $^{40}Ar/^{39}Ar$ Method: Oxford University Press, USA, 271 pp.

McLean, N.M., Bowring, J.F., and Bowring, S.A., 2011, An algorithm for U-Pb isotope dilution data reduction and uncertainty propagation: Geochemistry, Geophysics, Geosystems, v. 12, 26 p.

Miller, J.S., Matzel, J.E.P., Miller, C.F., Burgess, S.D., and Miller, R.B., 2007, Zircon growth and recycling during the assembly of large composite arc plutons: Journal of Volcanology and Geothermal Research, v. 167, p. 282-299.

Mills, R.D., and Coleman, D.S., 2013, Temporal and chemical connections between plutons and ignimbrites from the Mount Princeton magmatic center: Contributions to Mineralogy and Petrology, v. 165, p. 961-980.

Moran, S.C., Lees, J.M., and Malone, S.D., 1999, P wave crustal velocity structure in the greater Mount Rainier area from local earthquake tomography: Journal of Geophysical Research, v. 104, p. 10775-10786.

Mundil, R., Ludwig, K.R., Metcalfe, I., and Renne, P.R., 2004, Age and timing of the Permian mass extinctions: U/Pb dating of closed-system zircons: Science, v. 305, p. 1760-1763.

Parrish, R.R., and Krogh, T.E., 1987, Synthesis and purification of ^{205}Pb for U-Pb geochronology: Chemical Geology, v. 66, p. 103-110.

Parrish, R.R., Roddick, J.C., Loveridge, W.D., and Sullivan, R.W., 1987, Uranium-lead analytical techniques at the geochronology laboratory, Geological Survey of Canada: Geological Society of Canada Radiogenic Age and Isotopic Studies: Report 1, Paper 87-2, p. 3-7.

Rioux, M., Bowring, S.A., and Farmer, G.L., 2010, Timescales of emplacement and differentiation of shallow level plutons, the Organ Needle Batholith, New Mexico: Geological Society of America Abstracts with Programs, v. 42, n. 5, p.659.

Rosera, J.M., Coleman, D.S., and Stein, H.J., 2013, Re-evaluating genetic models for porphyry Mo mineralization at Questa, New Mexico: implications for ore deposition following silicic ignimbrite eruption: Geochemistry, Geophysics, Geosystems, v. 14, p. 1525-2027.

Schärer, U., 1984, The effect of initial ^{230}Th disequilibrium on young U-Pb ages: the Makalu case, Himalaya: Earth and Planetary Science Letters, v. 67, p. 191-204.

Schöpa, A., and Annen, C., 2013, The effects of magma flux variations on the formation and lifetime of large silicic magma chambers: Journal of Geophysical Research: Solid Earth, v. 118, p. 926-942.

Schilling, F.R., and Partzsch, G.M., 2001, Quantifying partial melt fraction in the crust beneath the Central Andes and the Tibetan Plateau: Physics and Chemistry of the Earth, v. 26, p. 239-246.

Seager, W.R., 1981, Geology of the Organ Mountains and southern San Andres Mountains, New Mexico: New Mexico Bureau of Mines and Mineral Resources Memoir 36, 97 p.

Seager, W.R., and Brown, L.F, 1978, The Organ Caldera: Field Guide to Selected Cauldron and Mining Districts of the Datil-Mogollon Volcanic Field, New Mexico: New Mexico Geological Society Special Publication No. 7, p. 139-149.

Seager, W.R., and McCurry, M., 1988, The cogenetic Organ Cauldron and Batholith, South Central New Mexico: evolution of a large-volume ash flow cauldron and its source magma chamber: Journal of Geophysical Research, v. 93, p. 4421-4433.

Smith, R.L., 1960, Ash flows: Geological Society of America Bulletin, v. 71, p. 795-841.

Smith, R.L., and Bailey, R.A., 1965, The Bandelier Tuff: a study of ash-flow eruption cycles from zoned magma chambers: IAV International Symposium on Volcanology, New Zealand, p. 83-103.

Tappa, M.J., Coleman, D.S., Mills, R.D., and Samperton, K.M., 2011, The plutonic record of a silicic ignimbrite from the Latir volcanic field, New Mexico: Geochemistry, Geophysics, Geosystems, v. 12, 16 p.

Verplanck, P.L., Farmer, G.L., McCurry, M., and Mertzman, S.A., 1999, The chemical and isotopic differentiation of an epizonal magma body: Organ Needle Pluton, New Mexico: Journal of Petrology, v. 40, p. 653-678.

Verplanck, P.L., Farmer, G.L., McCurry, M., Mertzman, S.A., and Snee, L.W., 1995, Isotopic evidence on the origin of compositional layering in an epizonal magma body: Earth and Planetary Science Letters, v. 136, p. 31-41.

Wendt, I., and Carl, C., 1991, The statistical distribution of the mean squared weighted deviation: Chemical Geology, Isotope Geoscience Section, v. 86, p. 275-285.

Yanicak, S.M., 1992, Petrology of silicic and syenitic faces of the Organ Needle Pluton, Organ Mountains batholith, Dona Ana County, southern New Mexico [M.S. thesis]: Las Cruces, New Mexico State University, 165 pp.

Zimmerer, M.J., and McIntosh, W.C., 2013, Geochronologic evidence of upper-crustal in situ differentiation: silicic magmatism at the Organ caldera complex, New Mexico: Geosphere, v. 9, p. 155-169.